International Journal of Nanomedicine

Dovepress

open access to scientific and medical research

Open Access Full Text Article

ORIGINAL RESEARCH

Magnesium-Doped Nano-Hydroxyapatite/Polyvinyl Alcohol/Chitosan Composite Hydrogel: Preparation and Characterization

Kui Zhang[1,*], Yan Liu[2,*], Zhenrui Zhao[1], Xuewen Shi[1], Ruihao Zhang[1], Yixiang He[1], Huaibin Zhang[1], Wenji Wang[3]

[1]The First Clinical Medical College of Lanzhou University, Lanzhou, People's Republic of China; [2]Department of Gynecology, First Affiliated Hospital of Xi 'an Medical College, Xi' an, People's Republic of China; [3]Department of Orthopedics, the First Hospital of Lanzhou University, Lanzhou, People's Republic of China

*These authors contributed equally to this work

Correspondence: Wenji Wang, The First Hospital of Lanzhou University, Lanzhou, 730000, People's Republic of China, Tel +86 13893221698, Email ldyyjzwwj@outlook.com

Background: Polyvinyl alcohol/Chitosan hydrogel is often employed as a carrier because it is non-toxic, biodegradable, and has a three-dimensional network structure. Meanwhile, Magnesium-doped nano-hydroxyapatite(Mg-nHA) demonstrated high characterization to promote the osteogenic differentiation of bone marrow derived mesenchymal stem cell(BMSCs). Therefore, in order to develop a porous hydrogel scaffold for the application of bone tissue engineering, an appropriate-type Mg-nHA hydrogel scaffold was developed and evaluated.

Methods: A composite hydrogel containing magnesium-doped nano-hydroxyapatite (Mg-nHA/PVA/CS) was developed using a magnetic stirring-ion exchange method and cyclic freeze-thaw method design, with polyvinyl alcohol and chitosan as the main components. Fourier transform infrared spectra (FTIR), electron energy dispersive spectroscopy (EDS), X-ray photoelectron spectrometer (XPS) and scanning electron microscopy (SEM) were employed to analyze the chemical structure, porosity, and elemental composition of each hydrogels. The equilibrium swelling degree, moisture content, pH change, potential for biomineralization, biocompatibility, the osteogenic potential and magnesium ion release rate of the composite hydrogel were also evaluated.

Results: SEM analysis revealed a well-defined 3D spatial structure of micropores in the synthesised hydrogel. FTIR analysis showed that doping nanoparticles had little effect on the hydrogel's structure and both the 5% Mg-nHA/PVA/CS and 10% Mg-nHA/PVA/CS groups promoted amide bond formation. EDS observation indicated that the new material exhibited favourable biomineralization ability, with optimal performance seen in the 5% Mg-nHA/PVA/CS group. The composite hydrogel not only displayed favourable water content, enhanced biocompatibility, and porosity (similar to human cancellous bone), but also maintained an equilibrium swelling degree and released magnesium ions that created an alkaline environment around it. Additionally, it facilitated the proliferation of bone marrow mesenchymal stem cells and their osteogenic differentiation.

Conclusion: The Mg-nHA/PVA/CS hydrogel demonstrates significant potential for application in the field of bone repair, making it an excellent composite material for bone tissue engineering.

Keywords: magnesium-doped nano-hydroxyapatite, polyvinyl alcohol, chitosan, hydrogel, physical crosslinking

Introduction

Hydrogel, a hydrophilic polymer with a three-dimensional reticular structure, is widely used in biomedical fields such as wound dressing, drug delivery, and tissue engineering.[1–3] Chitosan(CS) is the only natural cationic polysaccharide characterized by a linear semi-crystalline structure that can be enzymatically degraded into glucosamine by lysozyme without any toxic effects on the human body.[4–6] However, chitosan-based hydrogels have certain limitations due to their strong intermolecular hydrogen bonding force which results in brittleness and poor mechanical properties.[7] Polyvinyl

Received: 5 August 2023
Accepted: 12 January 2024
Published: 20 January 2024

Graphical Abstract

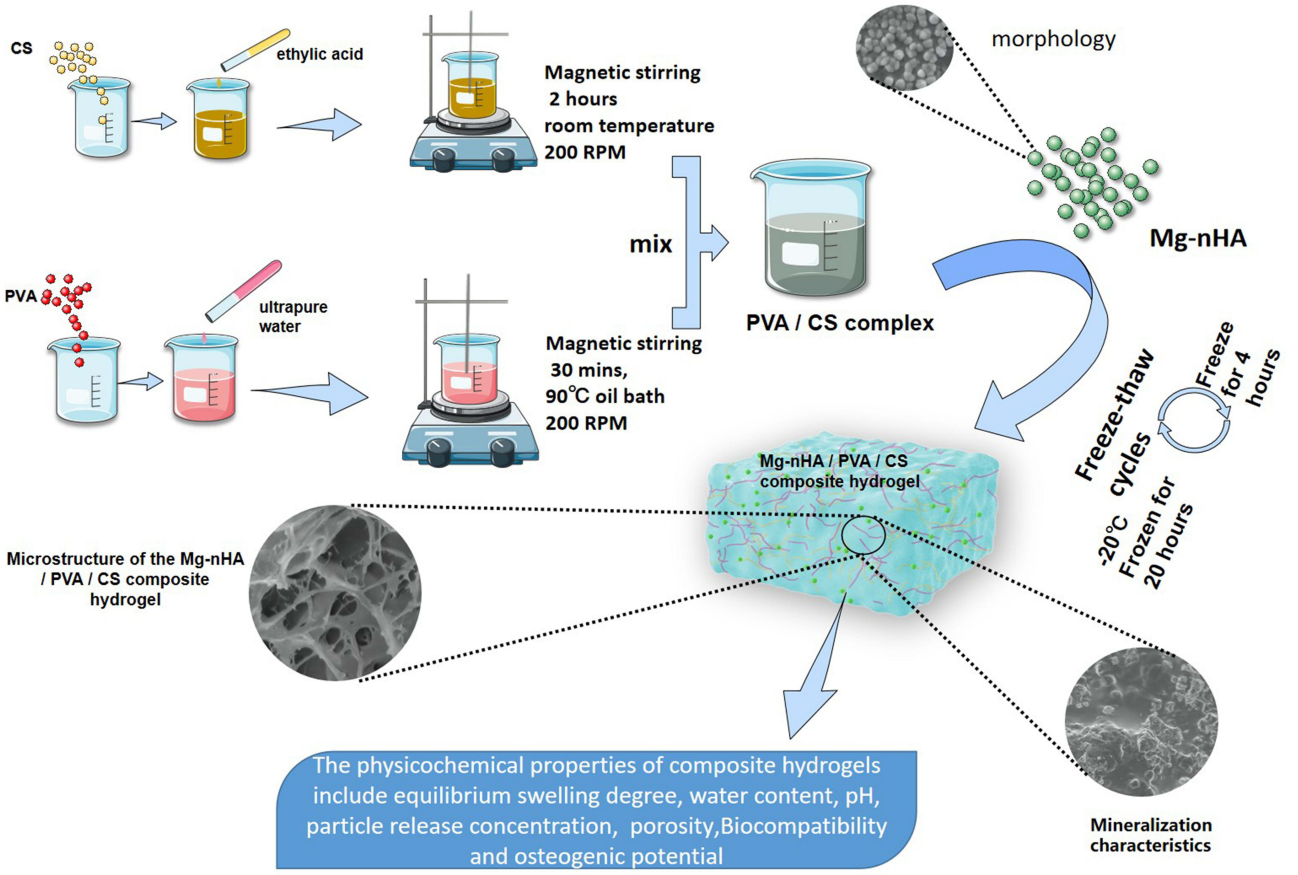

alcohol (PVA) monomer possesses hydroxyl groups that govern its physical and chemical properties while providing it with mechanical stability.[8,9] PVA can be combined with various polymers, metal ions, and biomolecules through diverse processing strategies to fabricate PVA-based composites exhibiting excellent mechanical properties, biocompatibility, and non-toxicity.[10–12]

PVA-based hydrogel can be prepared through chemical, physical, and radiation-induced cross-linking of PVA polymer chains.[13] Chemical cross-linking methods employ toxic agents such as glutaraldehyde, dye glycosides, or boric acids as crosslinker which are difficult to eliminate and trace residues may result in cytotoxicity.[14] Freeze-thaw (F-T)treatment enables dissolution of PVA hydrogel at high temperatures due to reversible physical cross-linking without the risk of cytotoxicity associated with the addition of cross-linking agents.[15] However, the brittleness and poor toughness of F-T composite PVA/CS hydrogel significantly restricts its application in the biomedical field.[16] To enhance mechanical properties and functionality, hydrated polymers and doped nanoparticles have recently been incorporated into PVA/CS hydrogels.[17,18]

Nano-hydroxyapatite (nHA) is a highly promising option for bone regeneration due to its chemical composition and crystal structure, which closely resembles those of bone minerals.[13,14] However, nHA exhibits inferior mechanical properties with lower brittle and fatigue strength as well as lower fracture toughness.[15,16] In contrast, magnesium (Mg) possesses higher fracture toughness and Young's modulus that is more similar to those of bone.[17] Therefore, combining magnesium appears to be a favorable approach that leverages the advantages of both materials. Since magnesium is biologically inert, it is necessary to attach magnesium implants to adjacent tissues. If the Mg-containing implant is porous, new bone may grow inside it, creating a proper connection between the implant and the surrounding bone

tissue.[18,19] An ideal implant must possess biocompatibility, osteoconductivity, biodegradability, and suitable mechanical properties that enable it to function properly under loading conditions.[20]

In this study, we have developed a novel composite hydrogel - magnesium-doped nano-hydroxyapatite/polyvinyl alcohol/chitosan (Mg-nHA/PVA/CS) through a simple and cost-effective strategy. The composite hydrogel not only possesses a porous three-dimensional structure but also exhibits excellent physicochemical properties by combining the advantages of each monomer, thus providing novel biomaterials for bone defect repair and other biomedical applications.

Materials and Methods

Materials

Chitosan (deacetylation 95%, viscosity 100–200map.s), Magnesium chloride solution (1 mol/L) and acetic acid (GR, 99.8%) were purchased from Aladdin, China. PVA (molecular weight of 146,000–186,000, alcohol 99 +%) was purchased from Sigma-Aldrich. Nano-nano-hydroxyapatite (needle, 97%, particle size =20nm) was purchased from MacLean, China. Magnesium Assay Kit(BioAssay Systems, USA). Simulated body fluid (SBF) was purchased from solarbio, China. Phosphate Buffer (PBS) was purchased from biosharp, China. Ultrapure water was used in the preparation of aqueous solutions. All chemicals were used without further purification.

Hydrogel Synthesis

Preparation of Magnesium-Doped Nanohydroxyapatite

Magnesium-doped nano-hydroxyapatite composite (Mg-nHA) was prepared using the magnetic stirring-ion exchange method as follows:[21]

(1) 5 g of nHA was immersed in 50 mL of a 1 M magnesium chloride solution and stirred at room temperature on a magnetic stirrer, operating at 300 rpm, for 24 hours.

(2) After the designated time, Mg-nHA particles were obtained from the mixture through centrifugation at 10,000 rpm for 3 minutes. The unreacted precursor fraction was subsequently washed three to four times with ultra-pure water.

(3) The final precipitate was collected and subjected to calcination at 60°C for 12 hours, followed by grinding into fine powder using a mortar and pestle.

Prepare the Mg-nHA/PVA/CS Composite Hydrogel

The Mg-nHA/PVA/CS composite hydrogel was prepared using the physical cross-linking method of repeated freezing and thawing,[22–24] as illustrated in Figure 1. The specific steps were as follows:

(1) Weigh 1g of CS and dissolve it in 50 mL of a 1% (w/v) acetic acid solution using magnetic stirring at 200rpm for 2 hours to obtain a 2% (w/v) CS solution. Then, weigh 5g of PVA and dissolve it in 50 mL of ultra-pure water under the oil bath stirring at 90°C for 30 minutes to obtain a PVA solution with a concentration of 10% (w/v). Mix the above two solutions at a volume ratio of 1:1 to obtain a mixed PVA/CS solution, which is magnetically stirred for another two hours.

(2) Preparation of Mg-nHA/PVA/CS: An appropriate amount of Mg-nHA was accurately added to the mixed solution in step (1). After 1 hour of magnetic stirring and ultrasonic oscillation, the Mg-nHA was uniformly dispersed in the mixed solution to obtain a homogeneous Mg-nHA/PVA/CS mixture.

(3) Pour the mixed solution from step (2) into the 24-well plate, and then place the sample in the refrigerator at −20°C for 20 hours. After that, remove it from the refrigerator and thaw it at room temperature for four hours. Repeat this freezing and thawing process four times.

(4) The acetic acid was neutralized by titrating a small volume of 1% (w/v) NaOH solution into a 24-well plate and allowing it to soak for 12 hours. Subsequently, ultra-pure water was added and the pH was adjusted to neutrality in order to obtain composite hydrogel within different experimental groups.

Methods

The hydrogels were categorized into four groups based on the presence or absence of Magnesium-doped nano-hydroxyapatite and its concentration (group PVA/CS; group Mg-nHA/PVA/CS of a 1% (w/v); group Mg-nHA/PVA/CS of a 5% (w/v); group Mg-nHA/PVA/CS of a 10% (w/v)). Fourier transform infrared spectra (FTIR), electron energy

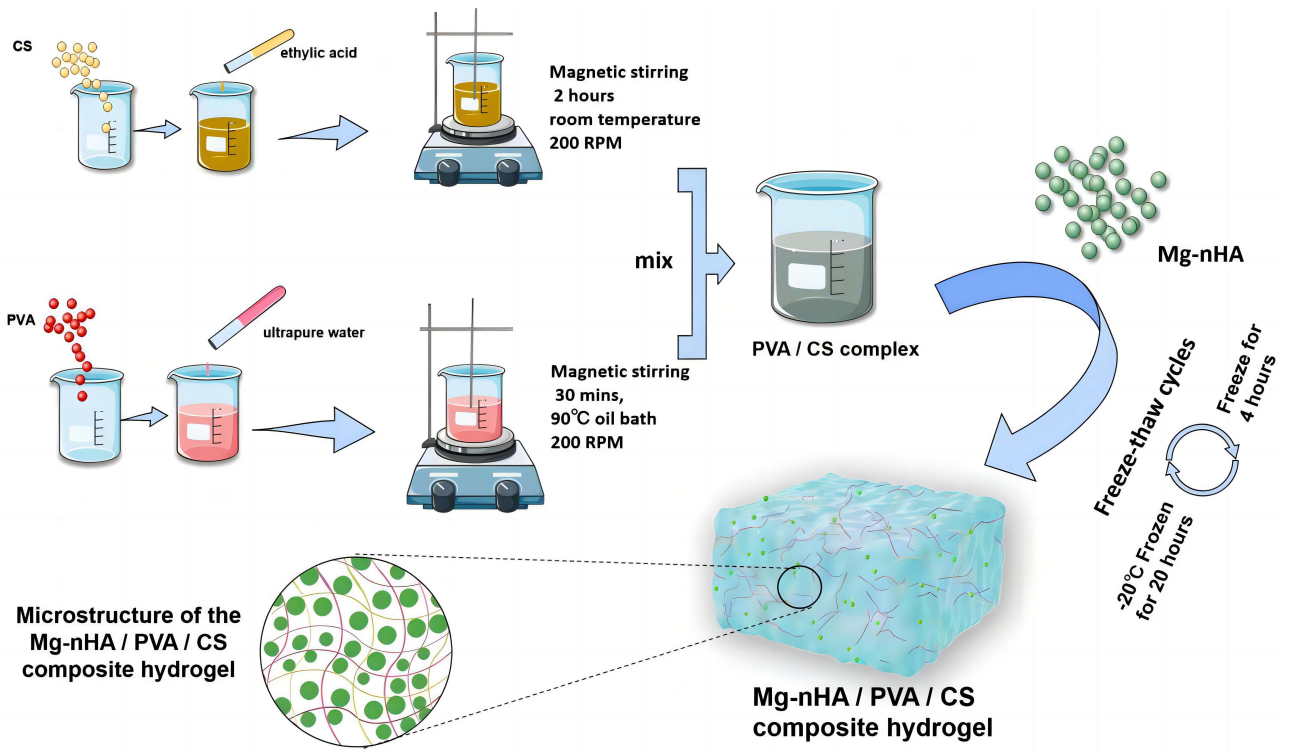

Figure 1 Schematic Illustration of the Fabrication and Microstructure of the Mg-nHA/PVA/CS composite hydrogel.

spectrometer (EDS), X-ray photoelectron spectrometer (XPS), and scanning electron microscope (SEM) were employed to analyze the chemical structure, porosity, and elemental composition of the hydrogel in each experimental group. The equilibrium swelling degree, moisture content, pH change, potential for biomineralization, biocompatibility, the osteogenic potential and magnesium ion release rate of the composite hydrogel were also evaluated. By comparing and analyzing the physical and chemical properties among different groups of new materials, the optimal ratio of nanoparticles doped in the hydrogel was determined.

Detection via Scanning Electron Microscopy

The morphology of the hydrogel was examined with a cold-field emission scanning electron microscope (SEM) (JSM-67101F, JEOL, Japan). After rapidly quenching the hydrogel in liquid nitrogen, it is transferred to a −20°C freeze dryer for 24 hours of lyophilization before removal. The resulting freeze-dried hydrogel samples were treated with gold spraying and characterized at an accelerating voltage of 15 kV. The nanoparticle particle size and hydrogel pore size were analyzed using Image J and Origin software.

Analysis of Porosity and Densitometry in the Hydrogels

The interconnect porosity of each sample was quantified using the liquid displacement method:[25,26] prior to immersion, the initial volume (V0) and weight (W0) were accurately measured, followed by submerging the sample in absolute ethanol for specific durations of 1, 3, 5, 7, 14, 28, 46, and 60 minutes. The samples were weighed at each time point until a stable weight was achieved and recorded as W1. The porosity (%) and density of the sample were calculated using the following formulas:[25] Porosity (%) = (W0 - W1)/(pV0) × 100% (where p represents the density of ethanol), while hydrogel density d was determined by dividing W0 by V0.

The Equilibrium Swelling Degree of the Hydrogels

In order to detect the equilibrium swelling degree of hydrogels,[27] the hydrogel was freeze-dried, weighed M_1, and then put it into ultra-pure water, and removed the gel at different time points such as 1.3,5,7,14,28,46,60 minutes, remove the

surface moisture of the swelling hydrogel with absorbent paper and weighed until the weight stabilized M_2. The equilibrium swelling ratio of the hydrogel was determined to use the formula (%) = $(M_2 - M_1)/M_1 \times 100\%$.[27]

The pH Variation of the Hydrogels

The hydrogel was placed in a centrifuge tube of phosphate-buffered saline (PBS) and incubated at 37°C for monitoring pH changes using a pH detector at various time points (0.5, 1, 3, 5, 10, 14, 20, 24 and 36 hours).

Ion Sustained-Release Detection of the Hydrogels

Different hydrogel groups were placed in bottles containing ultra-pure water and incubated at 37°C. At predetermined time intervals (5, 10, 15, 20, 25, and 30 days), the concentration of the magnesium ions in the hydrogel was examined and labeled as W1-W5. Rate of change of magnesium ion concentration W_X (%) = $(W_X\text{-}W_{X\text{-}1})/W_{X\text{-}1}\times100\%(2\leq x\leq5)$.

Fourier Transform Infrared Spectra (FTIR) of the Hydrogels

After the hydrogel was freeze-drying, the hydrogel composition was analyzed using Fourier transform infrared spectroscopy (Nicolet 170SX, Thermo Fisher Scientific Inc., USA) in the range of 400–4000 cm^{-1} with a resolution of 4 cm^{-1}. The spectral analysis of the four hydrogels was conducted over a range of 128 times, and subsequently, the alterations in functional groups among these four hydrogel groups were compared and analyzed.

Energy Spectrometer Scanning(EDS) Analysis of the Hydrogels

The freeze-dried hydrogel was analyzed using an X-ray energy chromatographer (EDS, Oxford Instruments, UK) to comprehensively explore the distribution and content of C, O, Mg and P elements in both the PVA/CS group and the Mg-nHA/PVA/CS group through point and mapping analysis. A comparative study was conducted to verify successful doping of Mg-nHA nanomaterials in the hydrogel.

The Moisture Content of the Hydrogels

The procedure for determining the water content of the hydrogel is briefly outlined as follows:[28] The hydrogel was first subjected to surface water removal using absorbent paper and weighed as W1. Subsequently, it was placed in a drying box at 70°C for different time intervals (0.5, 1, 3, 5, 7, 14, 28, 46, and 60 minutes) until reaching a constant weight of W2. The formula for calculating water content is expressed using the following formula: the rate of water content(%) = $(W_1 - W_2)/W_1 \times 100\%$.[28]

The Biomineralization Properties of the Hydrogels

The sterilized hydrogel was immersed in simulated body fluid (SBF) at a constant temperature of 37°C throughout the entire process within a controlled chamber. During the course, the SBF solution was renewed every other day to ensure maintenance of the essential environmental conditions necessary for mineralization. After a 14-day incubation period, the hydrogels were carefully extracted and subjected to three consecutive washes with ultra-pure water in order to completely eliminate any traces of adsorbed inorganic salts on the sample surface. Subsequently, freeze-drying was performed, followed by an analysis of the element composition and content of the hydrogel using Scanning Electron Microscopy (SEM) and X-ray photoelectron spectrometer (XPS).

In vitro Bone Mineralization Properties of Hydrogels

To further verify the bone mineralization properties of the hydrogel, we conducted experiments at the cellular level using in vitro cultured rat bone marrow mesenchymal stem cells (rBMSCs) (AW-YCR006 provided by Abiowell Biotechnology Co., Ltd) to detect bone mineralization. Alkaline phosphatase (ALP) staining and alizarin red staining were employed to evaluate the hydrogel's effect on bone mineralization visually. The extraction solution was prepared following Huang et al's experimental method.[29] Specifically, PVA/CS, 1% Mg-nHA/PVA/CS, 5% Mg-nHA/PVA/CS, and 10% Mg-nHA/PVA/CS hydrogels were individually immersed in rBMSC-specific medium (AW-MC025, Abiowell, China). After soaking at 37 °C and 100rpm for 24 hours, the extract was collected and filtered through a sterile 0.22μm filter to obtain a sterile extract. Finally, the collected extract was mixed with fresh rBMSC-specific medium at a ratio of 1:9 to form conditioned medium which was then stored in a refrigerator at 4°C.

Alkaline Phosphatase Staining

The rBMSCs was seeded in a 24-well plate at a density of 1×10^4 cells per well and cultured using a dedicated rBMSCs medium. After 24 hours of incubation, until the cells were fully adherent, the medium was aspirated, replaced with conditioned medium under different conditions, and continued for rBMSCs. They were cultured for 7 and 14 days in cell culture incubators. The ALP staining was performed according to the BCIP/NBT alkaline phosphatase chromogenic kit (PW0078, Beijing Leagene Biotechnology Co., Ltd.) instructions. The specific operations are as follows: (1) Discard the original culture medium in the 24-well plate and wash it three times with PBS for a duration of three minutes each; (2) Remove PBS and add 4% paraformaldehyde fixative solution, allowing it to incubate for 30 minutes; (3) Prepare a working solution of BCIP/NBT by mixing 10.1 mL of ALP Color Buffer, 33 μL of BCIP Solution (300×), and 66 μL of NBT Solution (150×). Ensure thorough mixing while avoiding exposure to light; (4) Remove the remaining PBS and add 400 μL of BCIP/NBT staining working solution to each well, ensuring complete coverage; (5) Incubate at room temperature for two hours; (6) Remove the BCIP/NBT staining working solution and terminate the chromogenic reaction by washing twice with steamed water before observing and photographing under an inverted microscope.

Servicin Red Staining

The rBMSCs were seeded in 24-well plates at a density of 1×10^4 cells per well and cultured using a dedicated rBMSCs medium. After 24 hours of incubation to allow for full cell adherence, the medium was aspirated and replaced with conditioned medium under different experimental conditions, which was then used for continued culture of rBMSCs. The cells were incubated for 14 days, followed by Alizarin Red staining according to the instructions provided in the Alizarin Red staining kit (G1450, Solarbio, China). The specific steps involved: (1) removal of the original culture medium from the 24-well plates and washing with PBS three times for a duration of three minutes each; (2) discarding PBS and adding 4% paraformaldehyde fixative for fixation lasting 30 minutes; (3) removal of fixative and further washing with PBS three times; (4) addition of 0.4 mL per well of a solution containing 2% Alizarin Red stain, ensuring complete coverage of the plate surface, followed by staining at room temperature for 30 minutes; (5) discarding the dye solution and washing with PBS three times before observing cell mineralization staining under an inverted microscope and capturing images.

Biocompatibility of the Hydrogels

To test the in vitro biocompatibility of synthetic hydrogels, cell counts were first performed and 3000 rBMSCs per well were seeded into a 96-well plate. After 24 hours of culture, after the cells were completely attached, the medium was aspirated and replaced with the conditioned medium of each group (90 microliter of special rBMSCs medium + 10 microliter of extract), and continuing the incubation under the above conditions. For the following 1.3, and 5 days, the medium was aspirated and 10 microliter containing 10% CCK-8 (C0037, Beyotime, China) and 90 microliter of medium were added to each well. Cell proliferation was calculated by measuring the absorbance at 450 nm of the supernatant after a further 2 h incubation in a 37 °C cell culture incubator. The cell viability was calculated using the following formula: Cell viability (% of control) = (OD of experimental group - OD of blank group) / (OD of control group - OD of blank group) x 100%.

Results and discussion

Magnesium-Doped Nano-Hydroxyapatite

Magnesium-doped nano-hydroxyapatite was synthesized through magnetic stirring-ion exchange. SEM characterization of Mg-nHA revealed evenly distributed nanoparticles with bright edges, areas with light centers, and minimal adhesion, displaying irregular spherical particles on the surface (Figure 2B). Subsequently, the mean size of the nanoparticles was determined and analyzed using ImageJ and Origin software, resulting in a value of (40.004±9.771) nm (Figure 2D). The SEM characterization of nHA nanoparticles showed that the nanoparticles were needle-like cylinders of length (83.882 ± 20.079) nm and width (33.165 ± 9.042) nm (Figure 2A and C).

Through an ion substitution method, calcium ions replace some magnesium ions in the magnesium chloride solution with nano-hydroxyapatite, resulting in the formation of Mg-nHA nanoparticles.[30,31] The introduction of magnesium ions induces a transformation in the morphology of the nanoparticles, changing them from needle-shaped to spherical, likely

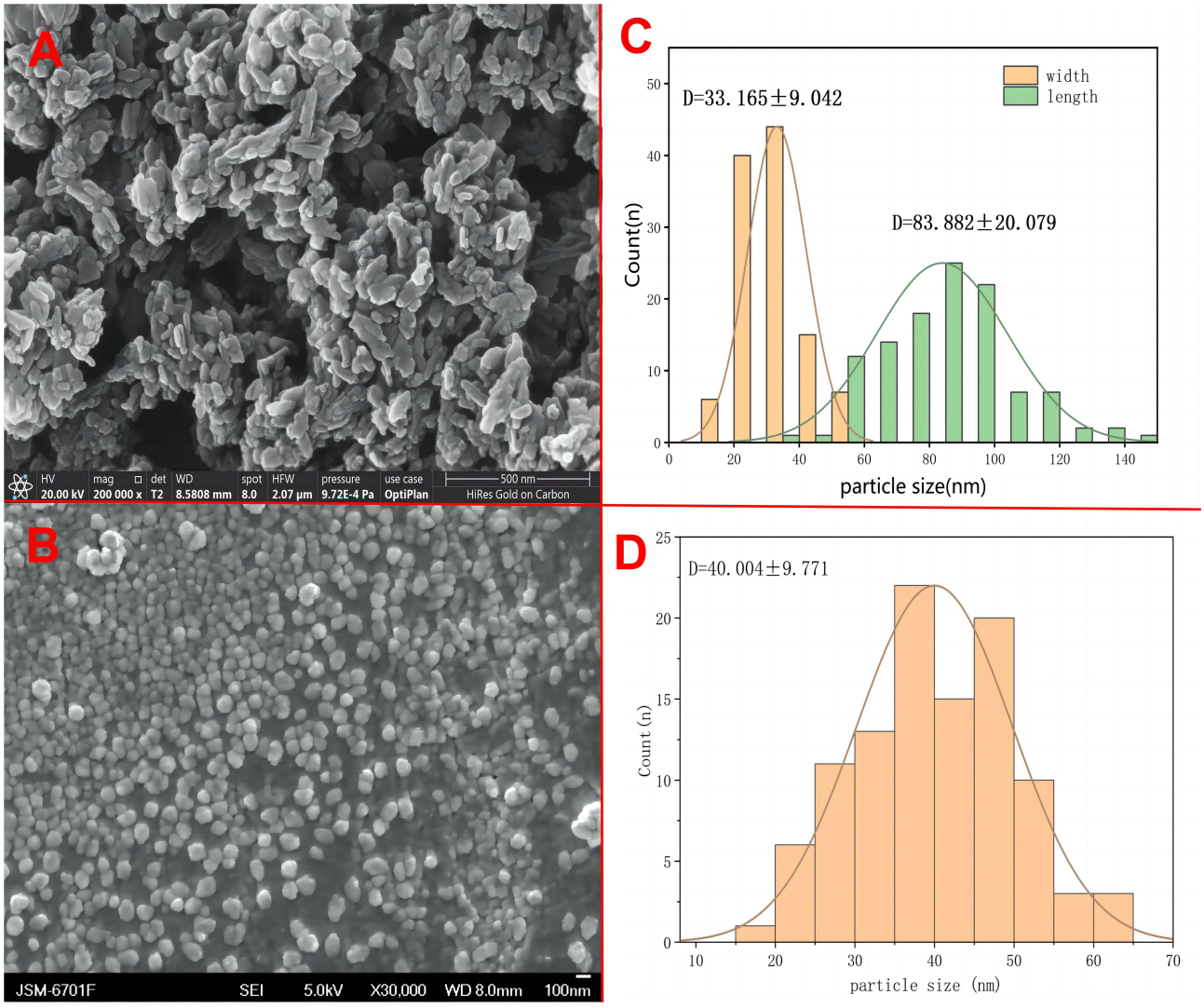

Figure 2 SEM images of nHA(**A**) and Mg-nHA(**B**), Histogram of statistical analysis of particle size of nHA(**C**) and Mg-nHA(**D**) according to the SEM plot.

due to alterations in their structure. Simultaneously, the mean particle size also increased, although it did not exceed 100nm, thus establishing a foundation for incorporating composite nanoparticles into the hydrogel.

Composite Hydrogel of Mg-nHA/PVA/CS

The Mg-nHA/PVA/CS composite hydrogels were prepared by physically cross-linking them using a repeated freeze-thaw method. From the appearance, it is evident that the transparency of the PVA/CS group gradually decreases compared to that of the 1% Mg-nHA/PVA/CS group, followed by the 5% Mg-nHA/PVA/CS group and finally, the 10% Mg-nHA/PVA/CS group. Additionally, there is a gradual shift in color from light white to dark white, while the edge of the hydrogel transitions from clear to slightly blurred (Figure $3A_{i\text{-}iv}$). The scanning electron microscopy analysis revealed that the four hydrogel groups exhibited a distinctive three-dimensional spatial structure (Figure $3C_{i\text{-}iv}$), which facilitates nutrient transportation, as well as the cell attachment and proliferation. The test results demonstrate that the PVA/CS group has significantly larger aperture sizes with greater spacing between apertures, while the diameter of individual holes is also larger. In contrast, the doped nanoparticle hydrogel group displays a layered three-dimensional structure with smaller individual hole diameters and minimal variation in aperture size. The pore sizes of each group were calculated and analyzed using Image J and Origin software, resulting in values of (0.606±0.263), (0.607±0.401), (0.412±0.223) and (0.355±0.234)

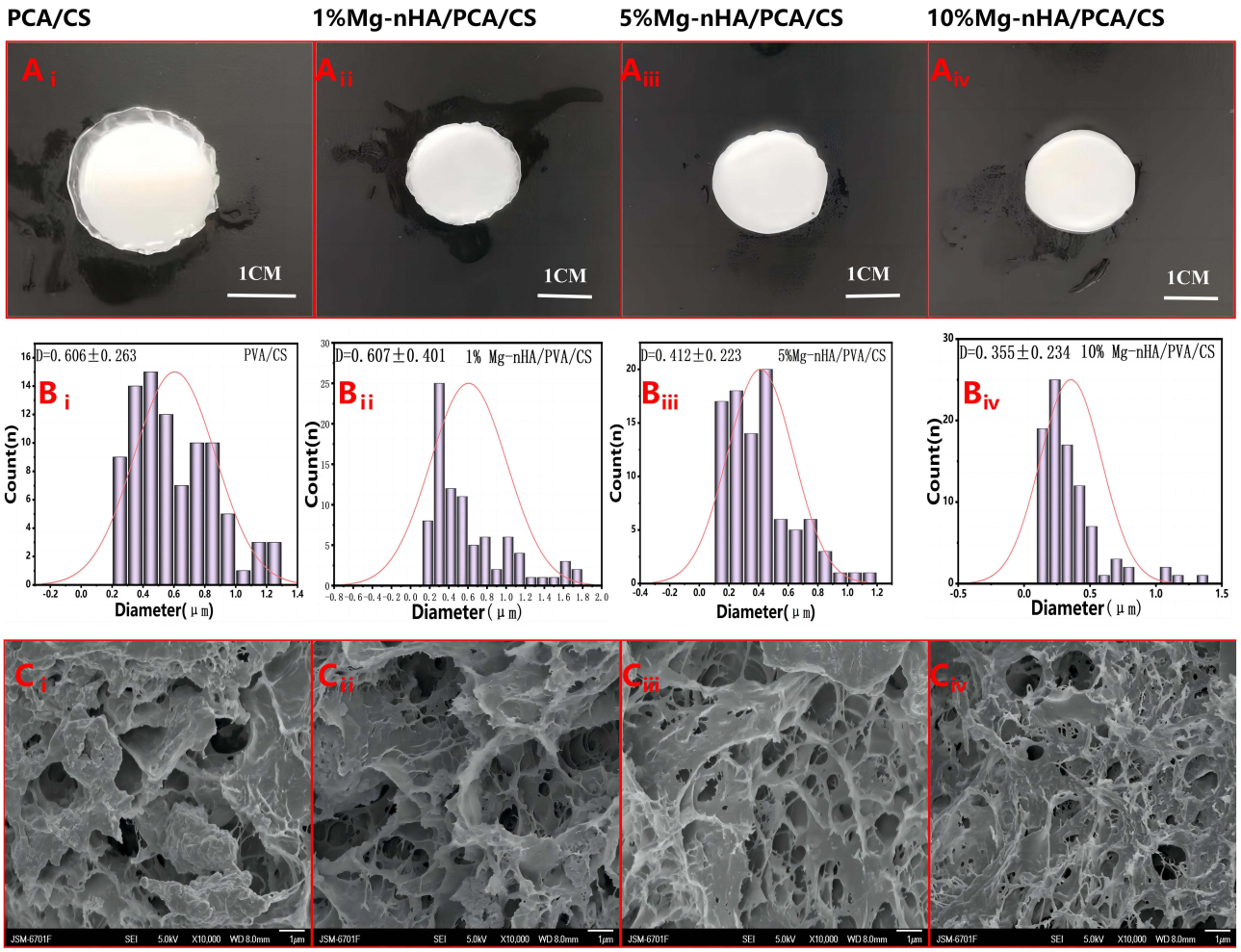

Figure 3 Macroscopic and microstructural features of composite hydrogels doped with different concentrations of Mg-nHA:PVA/CS hydrogel(**A_i**), 1%Mg-nHA/PVA/CS hydrogel(**A_{ii}**), 5%Mg-nHA/PVA/CS hydrogel(**A_{iii}**) and 10%Mg-nHA/PVA/CS hydrogel(**A_{iv}**) of macrostructure; Histogram of statistical analysis of aperture size of PVA/CS hydrogel(**B_i**), 1%Mg-nHA/PVA/CS hydrogel(**B_{ii}**), 5%Mg-nHA/PVA/CS hydrogel(**B_{iii}**) and 10%Mg-nHA/PVA/CS hydrogel(**B_{iv}**) according to the SEM plot; SEM pictures of PVA/CS hydrogel(**C_i**), 1%Mg-nHA/PVA/CS hydrogel(**C_{ii}**), 5%Mg-nHA/PVA/CS hydrogel(**C_{iii}**) and 10%Mg-nHA/PVA/CS hydrogel(**C_{iv}**).

μm, respectively, indicating a gradual decrease in average pore size with increasing doping amount (Figure $3B_{i\text{-}iv}$). During physical crosslinking, the hydrogels are doped with nanoparticles that establish robust ionic and hydrogen bonding interactions with the composite hydrogels.[32,33] This facilitates the assembly of PVA and CS polymer chains as a driving force, resulting in a reduction in pore size.

Semi-quantitative analysis of EDS energy spectrum elements was performed to detect the content of C, O, Mg, and P elements on the surfaces of the PVA/CS group and the Mg-nHA/PVA/CS group, Figure 4. The Point&ID analysis results of the energy spectrometer showed that the atomic content of elements in the hydrogel was as follows: PVA/CS group (C=63.14%, O=36.77%, Mg=0.07%, P=0.02%) and Mg-NHA/PVA/CS group (C=54.59%, O=39.09%, Mg=0.83%, P=5.49%). Point&ID diagram (Figure $4A_v$, B_v) of energy spectrometer showed that the content of magnesium and phosphorus in PVA/CS group was very low (0.02%, 0.07%, respectively), while the content of magnesium and phosphorus in Mg-nHA/PVA/CS group was significantly higher (0.83%, 5.49%, respectively). This may be the result of the nanoparticle Mg-nHA doping into the hydrogel. The Mapping analysis of the energy spectrometer revealed that the element particles in the Mapping map of each element exhibited discrete and uniform distribution characteristics. The color brightness of magnesium (Figure $4B_i$) and phosphorus (Figure $4B_{ii}$) Mapping maps of Mg-nHA/PVA/CS group were higher than that of PVA/CS group (Figure $4A_{i,\ ii}$), while the degree of elemental particle dispersion was lower. However, the C (Figure $4B_{iii}$) and O (Figure $4B_{iv}$) Mapping maps of the Mg-nHA/PVA/CS group showed relatively lower color

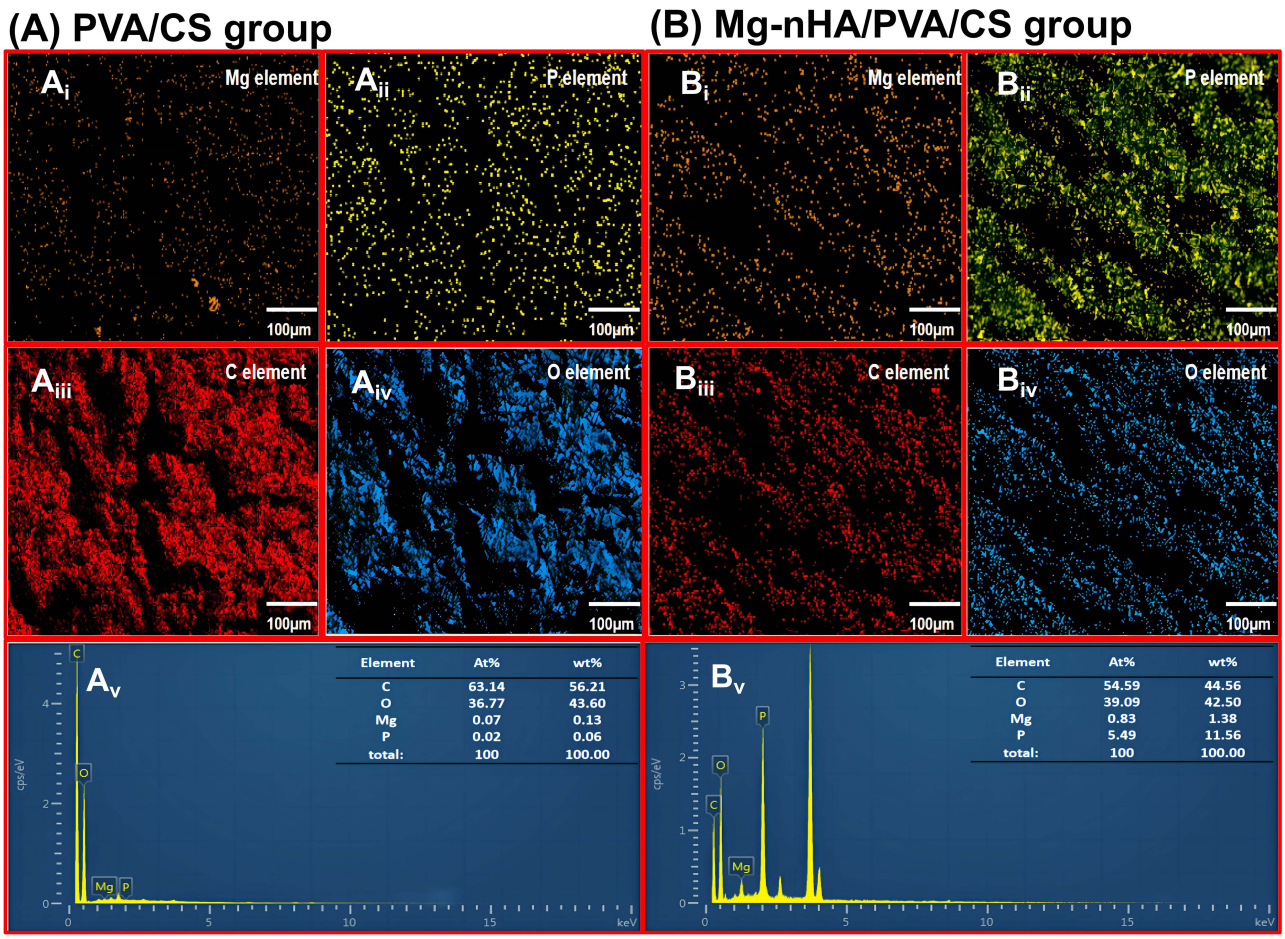

Figure 4 Distribution and content of surface elements in the PVA/CS hydrogel and the Mg-nHA/PVA/CS hydrogel by EDS: (**A**)Point&ID plot of Mg($\mathbf{A_i}$), P($\mathbf{A_{ii}}$), C($\mathbf{A_{iii}}$), and O ($\mathbf{A_{iv}}$) on the PVA/CS hydrogel surface and Maping plot($\mathbf{A_v}$) of the ratio of each element; (**B**)Point&ID plot of Mg($\mathbf{B_i}$), P($\mathbf{B_{ii}}$), C($\mathbf{B_{iii}}$), and O($\mathbf{B_{iv}}$) on the PVA/CS hydrogel surface and Maping plot($\mathbf{B_v}$) of the ratio of each element.

brightness but higher elemental particle dispersion compared to the PVA/CS group (Figure 4A$_{iii,\ iv}$). The results of energy spectrometer Mapping analysis showed that the brightness of Mg and P Mapping maps in the PVA/CS group was significantly lower than that in the Mg-nHA/PVA/CS group, which further confirmed the successful doping of Mg-nHA nanoparticles in the hydrogel. However, after energy spectrometer analysis, we found that the levels of magnesium and phosphorus in the PVA/CS group were extremely low, which could be attributed to various factors causing errors in instrument detection. For instance, samples might have come into contact with relevant elements during preparation and transportation, resulting in surface contamination. Alternatively, strong noise peaks during the detection process could have affected the accuracy of measurement. Additionally, residual magnesium and phosphorus on the sample preparation vehicle may have interfered with the test results. Moreover, deviations in measurement outcomes could also arise from the high sensitivity of the detection instrument.

To investigate the mechanism of Mg-nHA incorporation in PVA/CS hydrogel, we conducted FTIR analysis on each group after incorporation (Figure 5). The incorporation of Mg-nHA had a negligible impact on the primary structure of PVA/CS hydrogel, as depicted in Figure 5. This is evidenced by broad and intense peaks between 3000–3500 cm^{-1} corresponding to N-H and O-H stretching. The peak at 2940 cm^{-1} represents C-H stretching. Both PVA/CS and Mg-nHA/PVA/CS hydrogels exhibited a peak at 1650 cm-1, confirming amide I (C=O) expansion vibration. However, this observed peak gradually decreased from the PVA/CS group to the 10% Mg-nHA/PVA/CS group, indicating that the Mg-nHA concentration affects the amide bond formation.

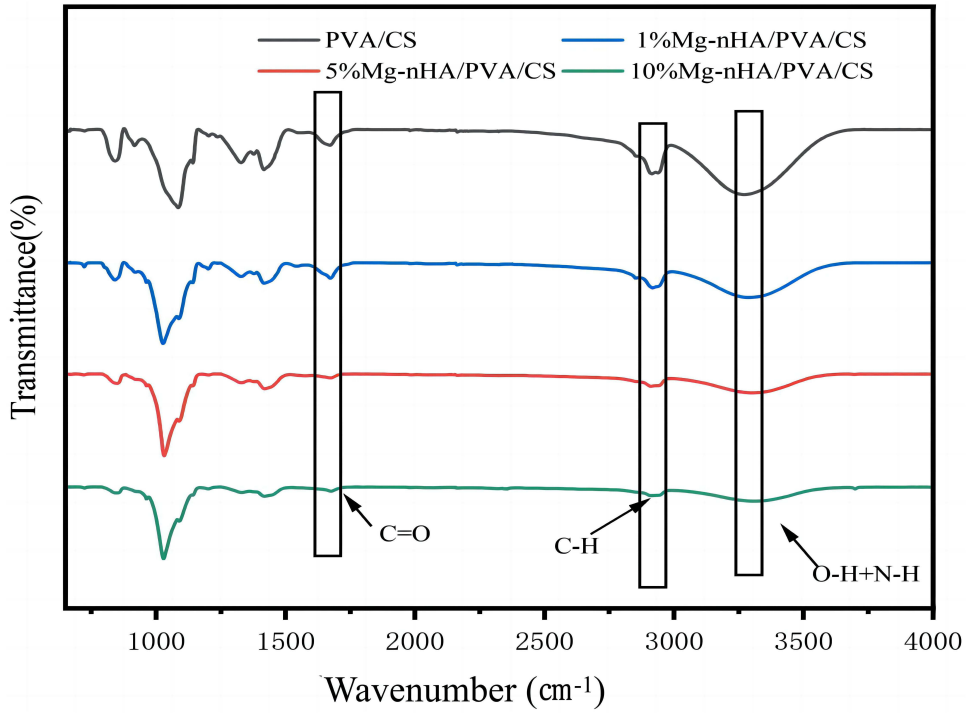

Figure 5 FTIR spectra of composite hydrogels doped with different concentrations of Mg-nHA.

Physical cross-linking plays a crucial role in hydrogel preparation due to its agent-free nature and simplified methodology, which helps avoid potential toxicity concerns associated with additive-induced experimental deviations.[34] Physical cross-linking often leads to the formation of polymer networks through chain entanglement, secondary forces, or molecular entanglement, such as hydrophobic interactions, hydrogen bonding, and ionic action[35-37] (Figure 6). However, the structures formed by these forces are more delicate and vulnerable to changes in temperature, pH, or ionic strength.[38]

The PVA/CS hydrogel was physically cross-linked to form pore structures that can spatially accommodate nanoparticles in a grid-like arrangement, resulting in varied physicochemical properties depending on the concentration of doped nanoparticles. Concurrently, it was observed that the introduction of doped nanoparticles had a negligible impact on the structural integrity of the hydrogel's functional groups, thereby preserving the advantageous physicochemical properties of PVA/CS hydrogel. Consequently, this composite hydrogel exhibits promising potential for diverse biomedical applications.

Porosity and Density

The porosity of each hydrogel group was determined by solvent displacement, as shown in Table 1. Porosity gradually increased from the PVA/CS to 10% Mg-nHA/PVA/CS groups (81.71%, 82.88%, 83.02%, and 86.3%, respectively). However, there were no statistically significant differences observed among these four groups. Meanwhile, based on the density calculation formula, the concentration of hydrogel increased from 0.89 mg/mL in the PVA/CS group to 1.04 mg/mL in the 10% Mg-nHA/PVA/CS group, indicating a positive correlation between nanoparticle content and hydrogel density. The obtained results are consistent with the SEM findings, suggesting that the interactions among reactive functional groups (-OH and -NH_2) of CS, the -OH group of PVA, and phosphate of Mg-nHA may influence the formation of porous structures.[39] This can lead to an increase in density of hydrogels and in porosity.

The porosity of human normal cancellous bone ranges from 50% to 90%,[40,41] and the porosity of four groups of doped hydrogels with varying nanoparticle content falls within this range. Mg-nHA/PVA/CS hydrogels can provide a spatial environment for the repair of cancellous bone that closely resembles the natural conditions found in the human

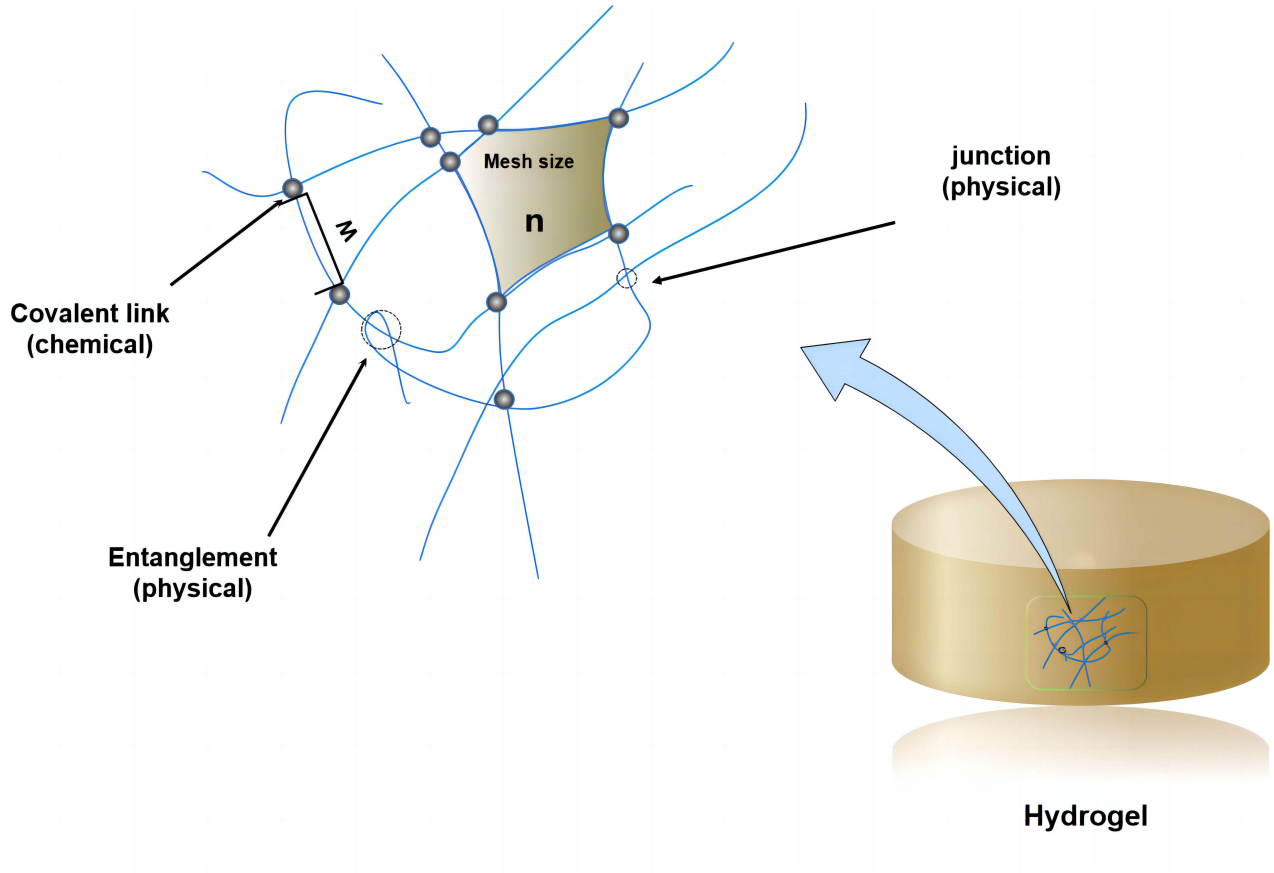

Figure 6 Structure of a crosslinked hydrogel: (n) the mesh size of hydrogel, (W) the average molecular weight between the cross-linking points.

body. This porous architecture promotes cellular adhesion and facilitates nutrient delivery to sites of tissue regeneration, as previously documented.[26] During SEM analysis, it was observed that these composites display microporosity with pore sizes ranging from 0.3 to 0.6 micrometers. This characteristic greatly increases their specific surface area, thereby enhancing both protein adsorption and nutrient delivery.[42] However, surface roughness enhances integrin-dependent attachment of osteocells and reduces pore size, which may affect the contact area between 3D structures and human tissue, thereby influencing cell migration within the 3D space.[43,44]

The Equilibrium Swelling Degree

The equilibrium swelling degree of each group hydrogel was determined by immersing it in ultra-pure water. As shown in Figure 7, the hydrogels of the 1% Mg-nHA/PVA/CS group, 5% Mg-nHA/PVA/CS group, and 10% Mg-nHA/PVA/CS group reached swelling equilibrium within 24 hours in extra-pure water, while it took as long as 48 hours for the PVA/CS

Table 1 The Porosity and Density of the Hydrogels in Each Group

Group	Porosity (%)	Density (g/cm^3)
PVA/CS	81.7103	0.8905
1%Mg-nHA/PVA/CS	82.8761	0.8907
5%Mg-nHA/PVA/CS	83.0190	0.9572
10%Mg-nHA/PVA/CS	86.3007	1.0395

Notes: PVA:polyvinyl alcohol; CS:Chitosan; Mg-nHA:Magnesium-doped nano-hydroxyapatite.

https://doi.org/10.2147/IJN.S434060 DovePress

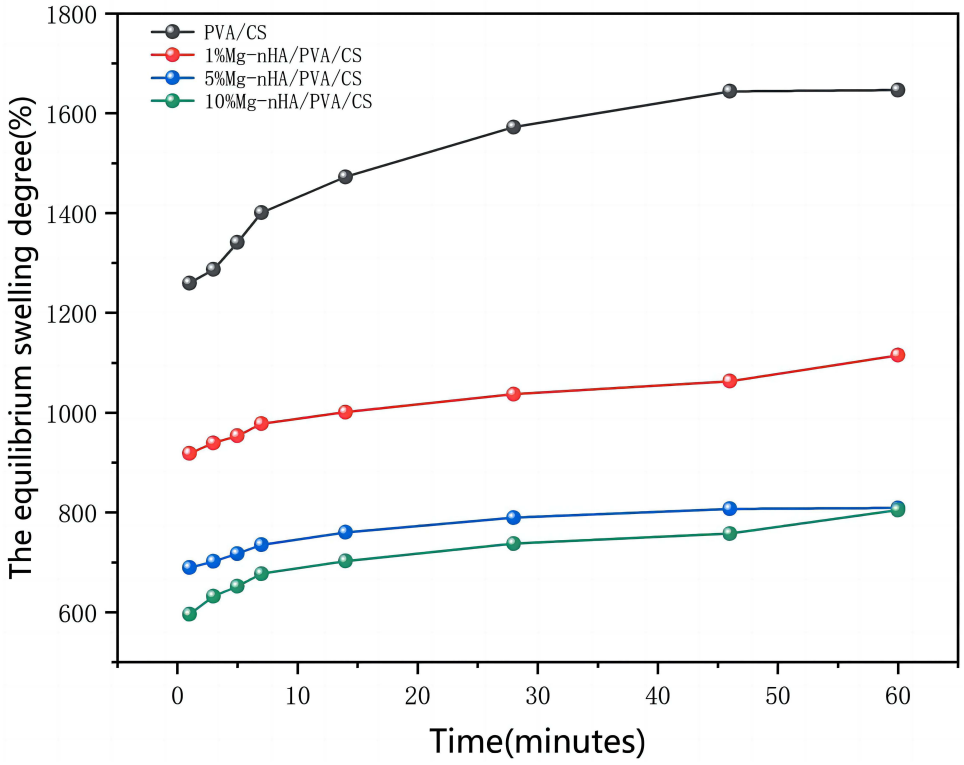

Figure 7 The equilibrium swelling degree of composite hydrogels doped with different concentrations of Mg-nHA.

group to reach such a state. Both the PVA/CS and 1% Mg-nHA/PVA/CS groups exhibited an equilibrium swelling degree exceeding 1000%, which was higher than that of the 5% Mg-nHA/PVA/CS group (809%) and the 10% Mg-nHA/PVA/CS group (804%).

The addition of extra nanoparticles to the hydrogel would reduce its hydrophilicity, while incorporating nano-Mg-nHA enhances the composite's stiffness but compromises its expansion properties.[45,46] Our findings align with those reported by Bhowmick et al.[47] The results demonstrate that an increase in the nanoparticles content leads to a decrease in water absorption capacity. In the presence of ultra-pure water, there is a significant influx of water molecules into the gel's free space due to the osmotic pressure difference between its interior and exterior. Experimental studies have shown that the presence of nanoparticles can alter the molecular structure of composite materials by cross-linking with CS on the polymer chain.[48] Additionally, it has been observed that water molecule diffusion within the polymer network also has a significant impact.

pH

The pH change of the hydrogel in a PBS solution was monitored using a pH detector. As shown in Figure 8, both the PVA/CS and 1% Mg-nHA/PVA/CS groups exhibited minimal changes in pH during the observation period of 36 hours, with their respective pH values remaining around 6.98 and 7.18 after immersion for five hours. The pH of the 5% Mg-nHA/PVA/CS group and the 10% Mg-nHA/PVA/CS group gradually increased over time, eventually stabilizing at approximately 8.7 after being immersed in PBS for 24 hours.

As depicted in the figure, the presence of magnesium ions induces the generation of an alkaline environment surrounding the hydrogel during its release process. With an increase in the concentration of magnesium ions within the hydrogel, there is a corresponding increase in alkalinity resulting from their activities, thereby leading to a rise in pH. The pH value of the 1% Mg-nHA/PVA/CS group remains close to 7, potentially due to the weak acid environment resulting from the pH (6.91) of the PBS stock solution and the alkaline byproducts generated by magnesium ions. Experimental investigations have demonstrated that the mildly alkaline environment promotes osteogenic differentiation and biomineralization.[49]

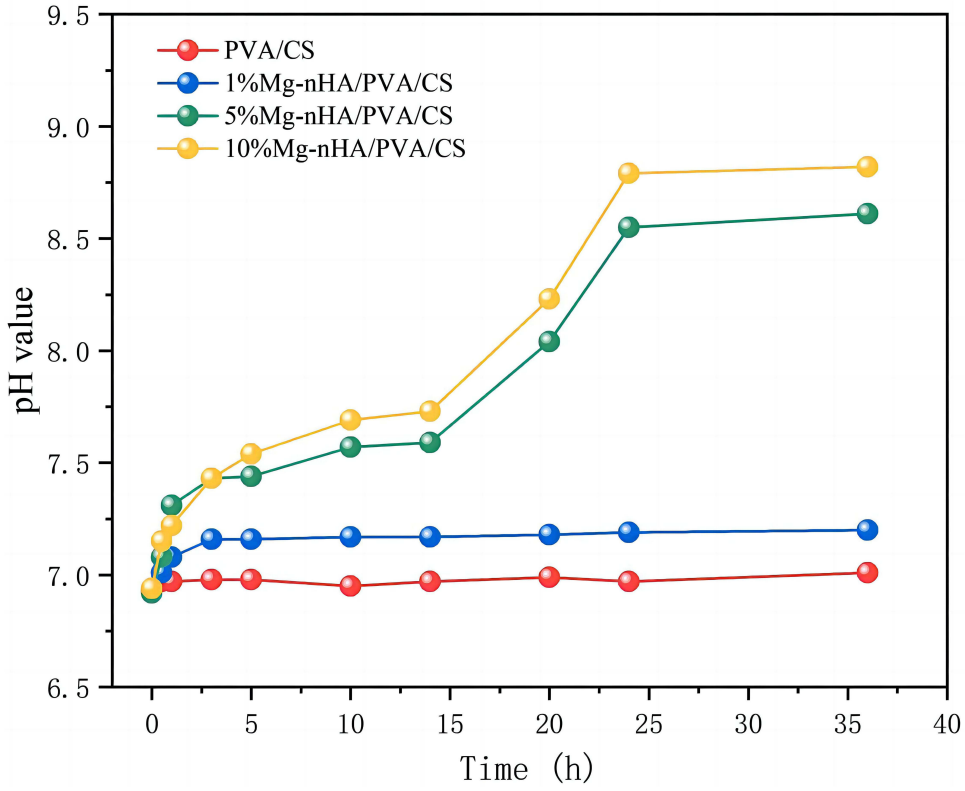

Figure 8 The pH change of composite hydrogels doped with different concentrations of Mg-nHA.

Performance of Ion Release

Mg^{2+} plays a crucial role in osteogenesis and mineralization, effectively promoting the formation and regeneration of bone matrix. As shown in Figure 9, in pure water, the hydrogels with three different concentrations of magnesium ions exhibited the highest release rate of magnesium ions after soaking for 10 hours. As time progressed, the release rate of magnesium ions gradually stabilized after 15 hours. Among the hydrogels with different concentrations, the 1% Mg-nHA/PVA/CS group showed the highest particle release rate at their respective time points, followed by the 5% Mg-nHA/PVA/CS group, while the 10% Mg-nHA/PVA/CS group demonstrated the lowest value. This difference may be attributed to a gradual reduction in pore size from 1% to 10% hydrogels, which affects the release rate of magnesium ions. Despite variations in release rates among groups, the release profile of Mg^{2+} in pure water is depicted in Figure 9, demonstrating similar trends among the three hydrogel groups with varying contents. This indicates their ability to sustain long-term and stable release of magnesium ions.

It has been determined that the optimal concentration range for magnesium ions is between 6 mmol/L and 10 mmol/L,[50] which significantly enhances the proliferation and osteogenic differentiation of bone marrow mesenchymal stem cells (BMSCs) by activating the MAPK/ERK signaling pathway.[51,52] The composite hydrogel synthesized in this study has long-term stable magnesium ion release characteristics, so it will have a positive impact on the application of bone tissue.

Moisture Content

During the determination of the water content in the hydrogel, the sample was subjected to vacuum drying, resulting in a gradual decrease in water over time until stabilization was achieved after 46 minutes (Figure 10). The moisture content difference of the four hydrogels showed minimal variation, ranging from 84% to 92%. Specifically, the water content of the hydrogel groups was as follows: PVA/CS group (92.25%), 1%Mg-nHA/PVA/CS group (89.87%), 5%Mg-nHA/PVA/CS group (87.21%), and 10% Mg-nHA/PVA/CS group (84.09%).

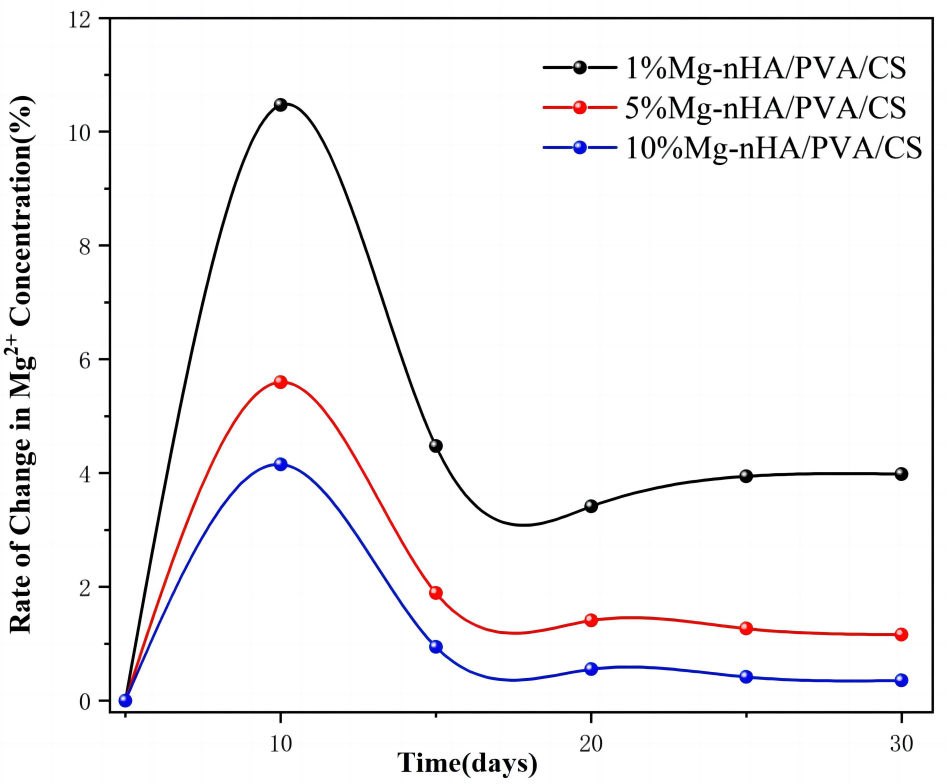

Figure 9 The rate of change in Mg^{2+} concentration of composite hydrogels doped with different concentrations of Mg-nHA.

Based on the findings from Figure 10, it was observed that all sample groups exhibited a continuous loss of water content in the hydrogel during vacuum drying over time. However, it was also noted that the 5% group displayed a relatively slower rate of weight change after 28 minutes, while the remaining three groups did not exhibit this behavior until after the 48-hour detection period. Several factors may contribute to this observation: (1) The sequential sampling and the weighing process during testing could introduce variations in sample weight at specific time points; (2) During sample heating, curling was observed due to the water loss, with varying degrees among different samples; this uneven heating might affect water evaporation rates on the sample surface; (3) The small weight of each sample group (A: 0.4862g; B: 0.4623 g; C: 0.4231 g; D:0.4763g) make them susceptible to slight influencing factors that can introduce bias into test results; (4) Since measurements of hydrogel weight changes were taken at specific time intervals (0.5, 1, 3, 5, 7, 14, 28, 46, and 60 min), there might be differences in water evaporation performance among groups initially and potentially better performance for the 5% group compared to others in terms of early-stage evaporation dynamics. The earlier change in water content within this group suggests further research is needed to verify its properties. However, the overall trend across all hydrogel groups remains similar. From a macro perspective, stability in weight changes after a detection period of 48 hours indicates near-complete volatilization of water from the hydrogels.

The lower water content of magnesium-doped nano-hydroxyapatite can be attributed to its smaller pore size, which results in less water being stored in the hydrogel. Additionally, the competitive hydrogen bonding between nanoparticles and water molecules within the polymeric chain contributes to a decrease in overall water molecule content. During freeze-thaw cycles, the intermolecular forces between polymeric chains weaken, resulting in a reduction of pore size within the three-dimensional network and a decrease in water content.[53]

In vitro Mineralization Properties

To evaluate the mineralization properties of the composite hydrogel in vitro, we immersed the samples in a simulated body fluid (SBF) solution to observe calcium and phosphorus deposition. After 14 days of immersion, we retrieved the

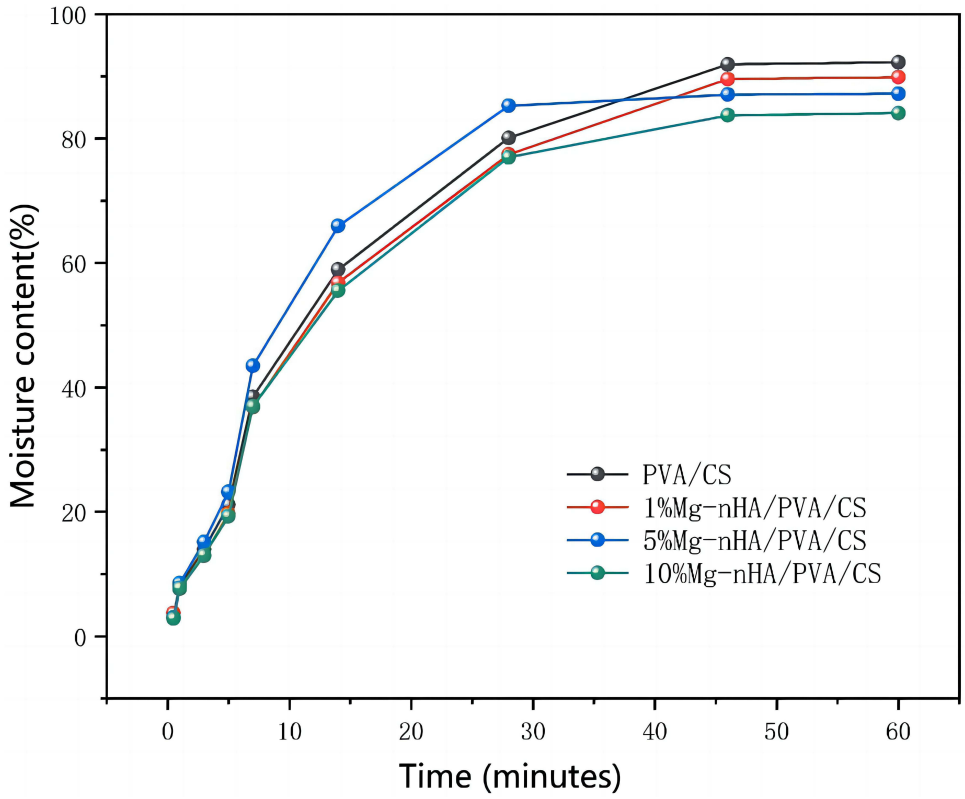

Figure 10 The water content of composite hydrogels doped with different concentrations of Mg-nHA.

mineralized hydrogel, freeze-dried it, and examined it under scanning electron microscopy (SEM). Additionally, semiquantitative elemental analysis was conducted using energy-dispersive X-ray spectroscopy (XPS) (Figure 11). As shown in Figure 11, the composite hydrogel group doped with nano-hydroxyapatite particles exhibited particle deposition on its surface. Among them, the 5%Mg-nHA/PVA/CS group showed the highest distribution of particles, while the 1% Mg-nHA/PVA/CS group displayed a lower distribution of particles (Figure 11$A_{i\text{-}iv}$). The variation in deposited phosphorus content was observed through elemental analysis (Figure 11$B_{i\text{-}iv}$). By using semi-quantitative analysis, the group of doped particles showed an increase in surface calcium and phosphorus content. The 1% Mg-nHA/PVA/CS group had a comparatively lower increase, while the 5% Mg-nHA/PVA/CS group displayed the highest relative atomic content with calcium and phosphorus contents of 1.31% and 1.24%, respectively. However, compared to the 5% Mg-nHA/PVA/CS group, the calcium and phosphorus content of the 10% Mg-nHA/PVA/CS group decreased(Figure 11C). The magnesium-containing hydroxyapatite content was lower in the 5% Mg-nHA/PVA/CS group compared to the 10% Mg-nHA/PVA/CS group; however, the XPS results were still higher in the former. In this section, the experimental purpose is to compare the mineralization potential of different groups of hydrogels through in vitro mineralization experiments, and the calcium, phosphorus content is used as an indirect indicator of the mineralization performance. In the 5% Mg-nHA/PVA/CS group, the phosphorus content was higher than that in the other groups, possibly because the hydrogel in the 5% Mg-nHA/PVA/CS group showed better mineralization properties. However, we should also see that the difference of calcium and phosphorus content between the 10% Mg-nHA/PVA/CS group and 5% group is small and not statistically significant, which may also be caused by the test error of the XPS test to detect the sample surface rather than the internal and external particle content of the sample.

To evaluate the bone mineralization properties of compound hydrogel in vivo, the authors observed the promotion of mineralization of rBMSCs by the culture of rBMSCs with ALP staining and alizarin red staining. ALP staining was performed on rBMSCs cultured in conditioned medium for 7 and 14 days (Figure 12). The results showed that at 7 days, the number of cells was small and the distribution was sparse under the microscope, and all cells showed different

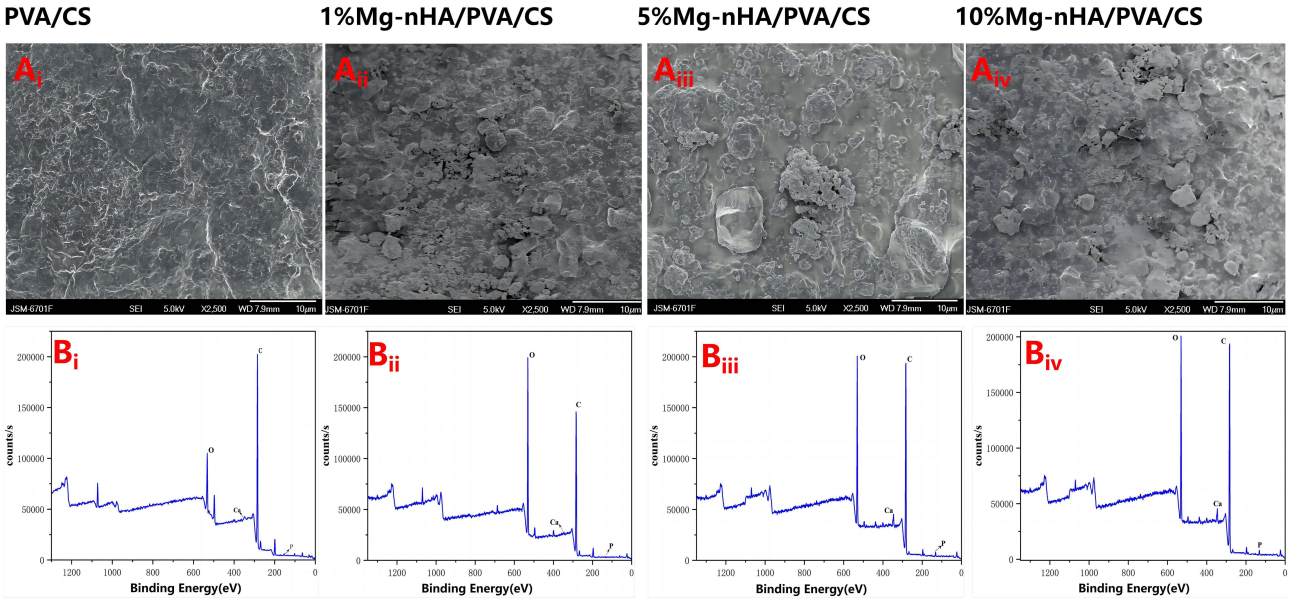

C

element	At (%)	element	At (%)	element	At (%)	element	At (%)
P	0.79	P	0.56	P	1.24	P	1.04
C	86.29	C	72.81	C	73.45	C	69.09
Ca	0.42	Ca	0.76	Ca	1.31	Ca	1.07
O	12.5	O	25.87	O	24.01	O	28.8
total	100	total	100	total	100	total	100

Figure 11 Macroscopic features of the composite hydrogels doped with different concentrations of Mg-nHA after SBF immersion by SEM and the content of surface elements in composite hydrogels with different Mg-nHA concentrations: PVA/CS hydrogel(**A_i**), 1%Mg-nHA/PVA/CS hydrogel(**A_{ii}**), 5%Mg-nHA/PVA/CS hydrogel(**A_{iii}**) and 10%Mg-nHA/PVA/CS hydrogel(**A_{iv}**) of macrostructure; (**B**)XPS pictures of PVA/CS hydrogel(**B_i**), 1%Mg-nHA/PVA/CS hydrogel(**B_{ii}**), 5%Mg-nHA/PVA/CS hydrogel(**B_{iii}**) and 10%Mg-nHA/PVA/CS hydrogel(**B_{iv}**); (**C**)content of surface elements in the PVA/CS hydrogel and the Mg-nHA/PVA/CS hydrogel by XPS.

degrees of purple staining. The ALP staining of cells in the Mg-nHA/PVA/CS hydrogel groups was deeper than that in the PVA group. At 14 days, the staining of all cells was darker than that at 7 days, and the cells were more concentrated and increased in number. In addition, at 14 days, the Mg-nHA/PVA/CS hydrogel groups had a significantly darker purple color than the PVA/CS group. In ALP staining, darker colors indicate stronger intracellular ALP activity. As ALP is one of the early markers in the process of bone mineralization, the hydrogel doped with nanoparticles had stronger ALP activity, and indirectly confirmed that the hydrogel doped with Mg-nHA could promote the bone mineralization process of rBMSCs. In addition, we performed alizarin red staining of rBMSCs cultured for 14 days (Figure 13). The results showed that the cell fluid of all rBMSCs appeared light red under the microscope. The outline of the cells was clearly visible, and a reddish mass of aggregated calcium nodules was also formed locally. Compared with the PVA/CS group, the Mg-nHA/PVA/CS hydrogel groups showed more light red clumps, which further confirmed that the Mg-nHA/PVA/CS hydrogel was able to promote the mineralization deposition of cellular matrix bone. Therefore, Mg-nHA/PVA/CS hydrogel may have promising applications in bone tissue engineering.

The nano-hydroxyapatite phosphates possess the capability to capture calcium ions in SBF fluid, thus aiding in the deposition of calcium and phosphorus and subsequently enhancing bone repair and biomineralization.[54] In this study, the hydrogel demonstrated a gradual and sustained release of magnesium ions and phosphate, supplying crucial components for bone tissue regeneration. Simultaneously, the liberation of magnesium ions facilitates the creation of a marginally alkaline milieu, thereby augmenting the mineralization characteristics of the hydrogel.

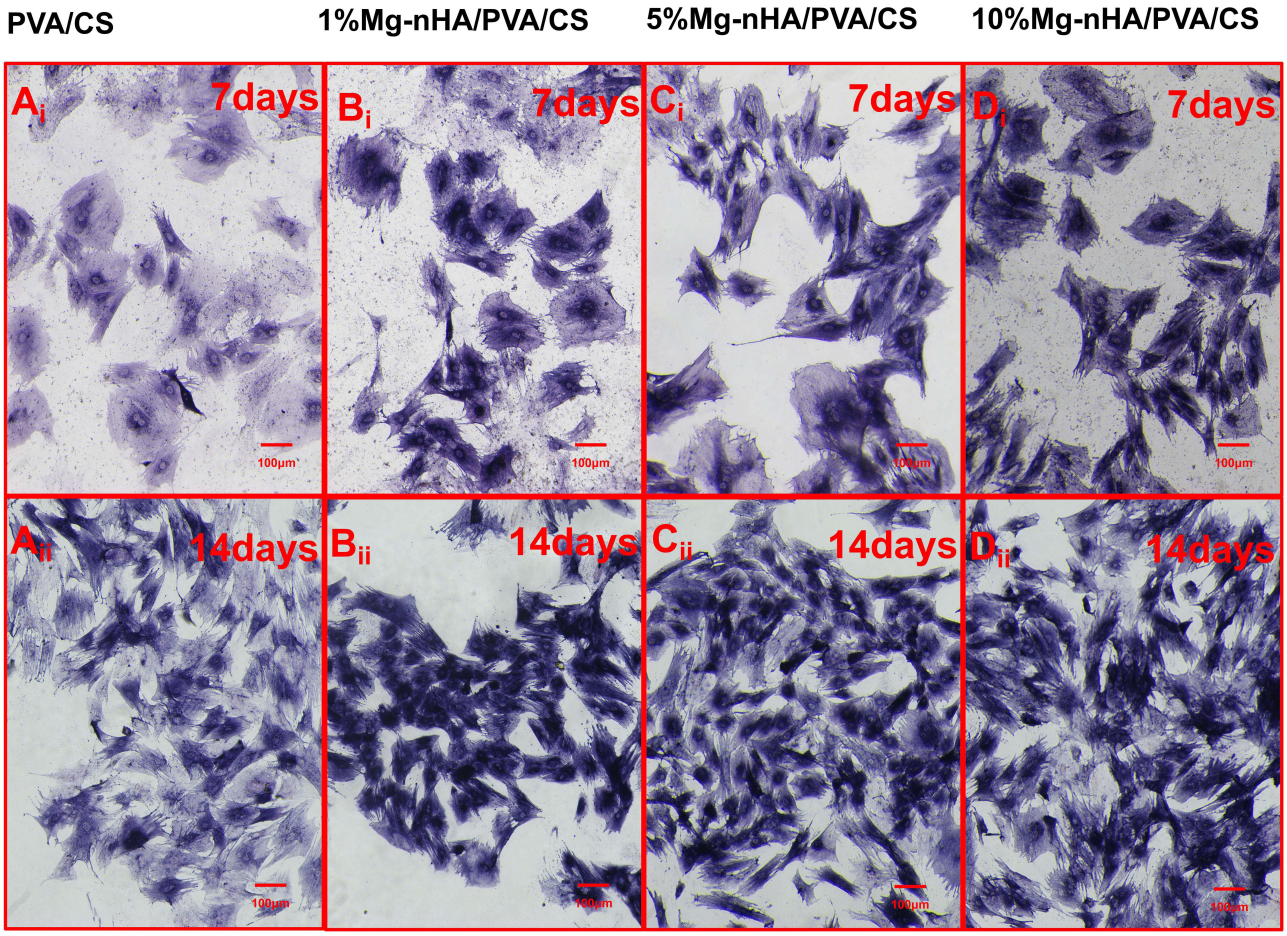

Figure 12 Images of ALP staining at 7 and 14 days after rBMSCs loading in the composite hydrogels doped with different concentrations of Mg-nHA: (**A**) ALP staining pictures of PVA/CS hydrogel in 7 days($\mathbf{A_i}$) and 14 days($\mathbf{A_{ii}}$); (**B**) ALP staining pictures of 1%Mg-nHA/PVA/CS hydrogel in 7 days($\mathbf{B_i}$) and 14 days($\mathbf{B_{ii}}$); (**C**) ALP staining pictures of 5%Mg-nHA/PVA/CS hydrogel in 7 days($\mathbf{C_i}$) and 14 days($\mathbf{C_{ii}}$); (**D**) ALP staining pictures of 10%Mg-nHA/PVA/CS hydrogel in 7 days($\mathbf{D_i}$) and 14 days($\mathbf{D_{ii}}$).

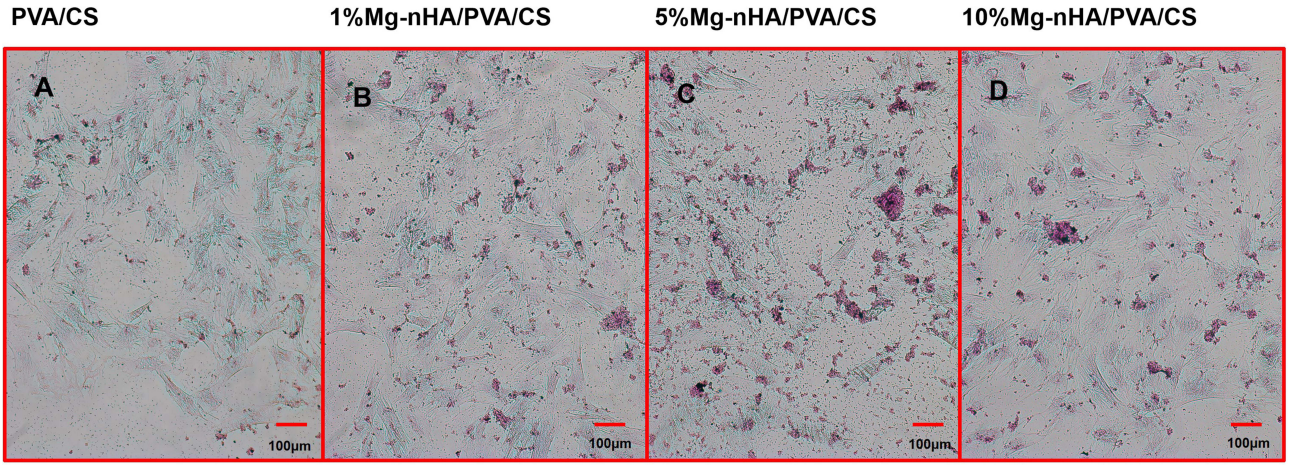

Figure 13 Images of alizarin red staining at 14 days after rBMSCs loading in the composite hydrogels doped with different concentrations of Mg-nHA: (**A**)PVA/CS hydrogel, (**B**)1%Mg-nHA/PVA/CS hydrogel, (**C**)5%Mg-nHA/PVA/CS hydrogel and (**D**)10%Mg-nHA/PVA/CS hydrogel.

Biocompatibility

After co-culturing with hydrogel extracts from each group for 1, 3, and 5 days, cell viability was assessed using the CCK-8 method, and the results are presented in Figure 14. As shown in Figure 14, after one day of co-culture, both the PVA/

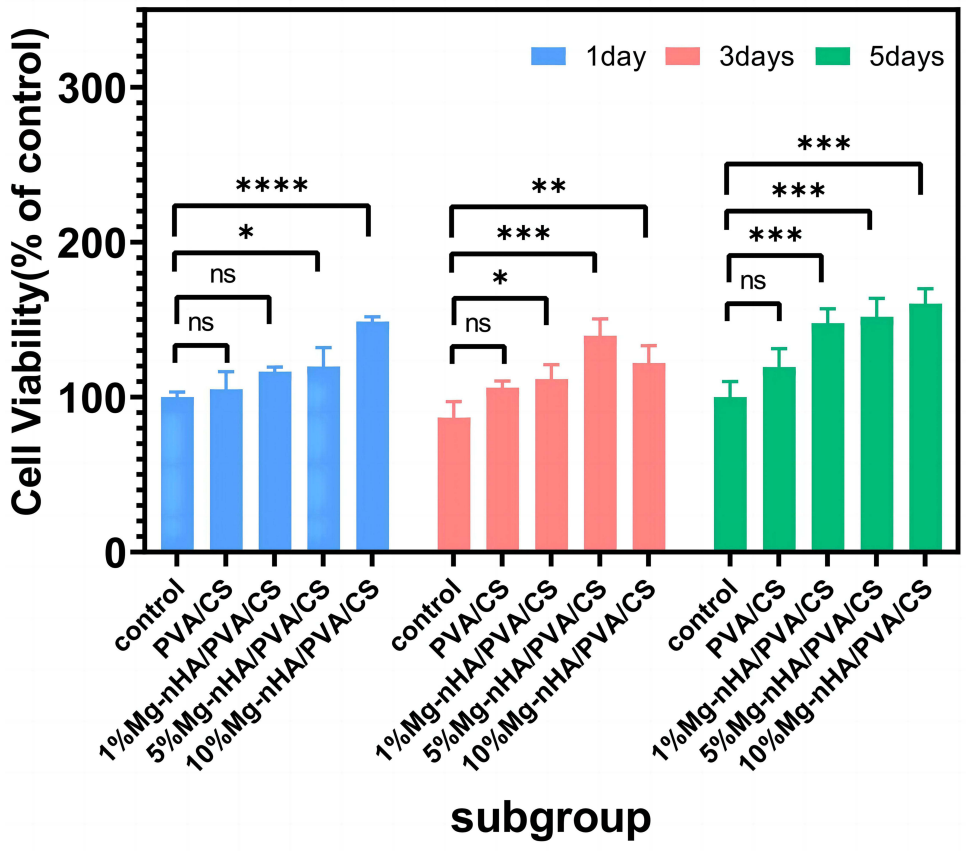

Figure 14 CCK-8 assay at 1, 3 and 5 days after rBMSCs loading in the composite hydrogels doped with different concentrations of Mg-nHA. (ns p>0.05, *p<0.05, **p<0.01, ***p<0.001, ****p<0.0001).

CS hydrogel group and the 1%Mg-nHA/PVA/CS hydrogel group exhibited a slight increase in cell viability compared to the control group; however, this difference was not statistically significant. In contrast, both the 5%Mg-nHA/PVA/CS hydrogel group and the 10%Mg-nHA/PVA/CS hydrogel group showed significantly higher cell viability than the control group with statistical significance. After three days of co-culture, there was an observed increase in cell viability within the PVA/CS hydrogel group; however, this difference did not reach statistical significance when compared to that of the control group. On the other hand, cell viability in all of the Mg-nHA-doped hydrogel groups was significantly higher than that in the control groups, with statistically significant differences. By the day five of co-culture period again an increase in cell viability within PVA/CS hydrogel groups could be observed; however, once more no statistically significant differences were found when compared to those seen within control groups. Nonetheless, it is worth noting that even at this time point Mg-nHA doped hydrogel groups still demonstrated higher levels of cell viability than their corresponding controls with these differences being statistically significant.

In Figure 14, we found that in the 1-day culture group, the 10% group contained more Mg-nHA, resulting in the rapid release of particles, which had a significant effect on cell proliferation. However, the 1% group had less effect on cell viability due to the less doped Mg-nHA and slower particle release, and although cell viability was increasing, there was no statistically significant difference. In the group co-cultured for 3 days, the 5% hydrogel group had the most significant effect on cell viability, which may indicate a better biocompatibility of the 5%Mg-nHA/PVA/CS hydrogel compared to the 1% and 10% hydrogels. As the time was extended to 5 days, the proliferation promotion effect of Mg-nHA/PVA/CS hydrogel group was still obvious. This fully indicates that the sustained release Mg^{2+} of composite hydrogel can effectively promote cell proliferation and significantly enhance cell viability. Additionally, the PVA/CS hydrogel group exhibited a modest enhancement in cell viability compared to the control group in the 1,3, and 5 days experimental groups; however, this difference was not statistically significant. Therefore, we conclude that the addition of

nanoparticles Mg-nHA to PVA/CS hydrogel can significantly enhance the cell activity and promote cell proliferation, showing good biocompatibility.

Conclusion and Deficiencies

The composite hydrogel of polyvinyl alcohol/chitosan, which contains magnesium-doped nanohydroxyapatite (Mg-nHA/PVA/CS), was fabricated using magnetic stirring-ion exchange and repeated freeze-thaw-physical cross-linking techniques. The doping of this nanoparticle does not significantly alter the functional of group structure in PVA/CS, thus allowing for the retention of favorable physicochemical properties in PVA/CS hydrogel. The porosity of Mg-nHA/PVA/CS composite hydrogel closely resembles that of normal human cancellous bone, which facilitates the replication of the microenvironment in human bone tissue. Additionally, the Mg-nHA/PVA/CS composite hydrogel exhibits favorable swelling properties and water absorption. The Mg-nHA/PVA/CS hydrogel releases magnesium ions gradually and consistently, creating an alkaline microenvironment that promotes osteogenic differentiation. Moreover, Mg-nHA/PVA/CS composite hydrogel not only has good biocompatibility, but also have peculiarity in vitro mineralization properties, which can enhance rBMSCs proliferation and osteogenic differentiation. The Mg-nHA/PVA/CS composite hydrogels show promising potential for application in the field of bone repair, making them a favorable composite material for bone tissue engineering applications.

However, it is important to acknowledge certain limitations. Firstly, the analysis of hydrogels' surface composition and structure using techniques like SEM, XPS, EDS, etc., restricts the comparison and analysis within the material's entirety, potentially impacting test results. Secondly, during physical and chemical property testing, samples often experience uneven heating leading to morphological changes that can introduce variations in results. Thirdly, real-world application environments such as temperature, humidity, and pressure may influence the material performance; however, further research is required for a comprehensive assessment of these effects. Fourthly, the aforementioned performance parameters are not the only ones to consider, other factors like electrical conductivity or optical properties are crucial for specific applications of hydrogel. Lastly, but importantly, if composite hydrogels are employed in biomedical applications, evaluating their biocompatibility becomes critical; this study only conducted a preliminary assessment without fully considering variances in response among different cell types or human tissues. These identified shortcomings highlight areas requiring the further improvement and extensive discussion in future research endeavors. Scientific inquiry is an ongoing process that necessitates providing comprehensive data with utmost accuracy and objectivity to enhance our understanding and application of scientific knowledge.

Data Sharing Statement

The data can be obtained either through the attachment or by contacting the corresponding author.

Consent for Publication

All authors agree to publish this paper in this journal.

Acknowledgments

We would like to express our gratitude to the free retrieval database platform provided by Lanzhou University Library, and extend our heartfelt thanks to Ruidi Biotechnology Co., Ltd. in Lanzhou City for providing us with a research platform.

Author Contributions

All authors made a significant contribution to the work reported, whether that is in the conception, study design, execution, acquisition of data, analysis and interpretation, or in all these areas; took part in drafting, revising or critically reviewing the article; gave final approval of the version to be published; have agreed on the journal to which the article has been submitted; and agree to be accountable for all aspects of the work.

Funding

There is no funding to report.

Disclosure

The authors declare that they do not have any known financial interests or personal relationships that could be perceived as exerting influence on the findings presented in this paper.

References

1. Chen X, Ji N, Li F, et al. Dual Cross-Linked Starch–Borax Double Network Hydrogels with Tough and Self-Healing Properties. *Foods*. 2022;11(9):1315. doi:10.3390/foods11091315
2. Rao KM, Narayanan KB, Uthappa UT, Park PH, Choi I, Han SS. Tissue Adhesive, Self-Healing, Biocompatible, Hemostasis, and Antibacterial Properties of Fungal-Derived Carboxymethyl Chitosan-Polydopamine Hydrogels. *Pharmaceutics*. 2022;14(5):1028. doi:10.3390/pharmaceutics14051028
3. Wang Q, Zhang Y, Ma Y, Wang M, Pan G. Nano-crosslinked dynamic hydrogels for biomedical applications. *Mater Today Bio*. 2023;20:100640. doi:10.1016/j.mtbio.2023.100640
4. Zhang P, Chen D, Li L, Sun K. Charge reversal nano-systems for tumor therapy. *J Nanobiotechnol*. 2022;20(1):31. doi:10.1186/s12951-021-01221-8
5. Woraphatphadung T, Sajomsang W, Rojanarata T, Ngawhirunpat T, Tonglairoum P, Opanasopit P. Development of Chitosan-Based pH-Sensitive Polymeric Micelles Containing Curcumin for Colon-Targeted Drug Delivery. *AAPS Pharm Sci Tech*. 2018;19(3):991–1000. doi:10.1208/s12249-017-0906-y
6. Kean T, Thanou M. Biodegradation, biodistribution and toxicity of chitosan. *Adv Drug Delivery Rev*. 2010;62(1):3–11. doi:10.1016/j.addr.2009.09.004
7. Zhang S, Wan Y, Yuan W, et al. Preparation of PVA-CS/SA-Ca(2+) Hydrogel with Core-Shell Structure. *Polymers*. 2022;14(1):212. doi:10.3390/polym14010212
8. Ngadiman NHA, Yusof NM, Idris A, Fallahiarezoudar E, Kurniawan D. Novel Processing Technique to Produce Three Dimensional Polyvinyl Alcohol/Maghemite Nanofiber Scaffold Suitable for Hard Tissues. *Polymers*. 2018;10(4):353. doi:10.3390/polym10040353
9. Tadesse MG, Lübben JF. Recent Progress in Self-Healable Hydrogel-Based Electroluminescent Devices: a Comprehensive Review. *Gels*. 2023;9(3):250. doi:10.3390/gels9030250
10. Gherman SP, Biliuță G, Bele A, et al. Biomaterials Based on Chitosan and Polyvinyl Alcohol as a Drug Delivery System with Wound-Healing Effects. *Gels*. 2023;9(2):122. doi:10.3390/gels9020122
11. Gao L, Hou Y, Wang H, et al. A Metal-Ion-Incorporated Mussel-Inspired Poly(Vinyl Alcohol)-Based Polymer Coating Offers Improved Antibacterial Activity and Cellular Mechanoresponse Manipulation. *Angewandte Chemie*. 2022;61(21):e202201563. doi:10.1002/anie.202201563
12. Zhu N, Ji H, Yu P, et al. Surface Modification of Magnetic Iron Oxide Nanoparticles. *Nanomaterials*. 2018;8(10):810. doi:10.3390/nano8100810
13. Chen Z, Liu Y, Huang J, et al. Influences of Process Parameters of Near-Field Direct-Writing Melt Electrospinning on Performances of Polycaprolactone/Nano-Hydroxyapatite Scaffolds. *Polymers*. 2022;14(16):3404. doi:10.3390/polym14163404
14. Zhang K, Zhu Y, Wang W. Application of nano-hydroxyapatite matrix graft in inter-vertebral fusion therapy: a meta-analysis. *BMC Musculoskeletal Disorders*. 2023;24(1):427. doi:10.1186/s12891-023-06405-x
15. Vaiani L, Boccaccio A, Uva AE, et al. Ceramic Materials for Biomedical Applications: an Overview on Properties and Fabrication Processes. *J Functional Biomaterials*. 2023;14(3):146. doi:10.3390/jfb14030146
16. Park JE, Jang YS, Bae TS, Lee MH. Biocompatibility Characteristics of Titanium Coated with Multi Walled Carbon Nanotubes-Hydroxyapatite Nanocomposites. *Materials*. 2019;12(2):224. doi:10.3390/ma12020224
17. Yusop AH, Bakir AA, Shaharom NA, Abdul Kadir MR, Hermawan H. Porous biodegradable metals for hard tissue scaffolds: a review. *Int J Biomater*. 2012;2012:641430. doi:10.1155/2012/641430
18. Grau M, Seiler C, Roland L, et al. Osteointegration of Porous Poly-ε-Caprolactone-Coated and Previtalised Magnesium Implants in Critically Sized Calvarial Bone Defects in the Mouse Model. *Materials*. 2017;11(1):6. doi:10.3390/ma11010006
19. Schiefer H, Bram M, Buchkremer HP, Stöver D. Mechanical examinations on dental implants with porous titanium coating. *J Mater Sci Mater Med*. 2009;20(8):1763–1770. doi:10.1007/s10856-009-3733-1
20. Khan S, Kumar V, Roy P, Kundu PP. TiO(2) doped chitosan/hydroxyapatite/halloysite nanotube membranes with enhanced mechanical properties and osteoblast-like cell response for application in bone tissue engineering. *RSC Adv*. 2019;9(68):39768–39779. doi:10.1039/c9ra08366a
21. Sihn Y, Yang HM, Park CW, Yoon IH, Kim I. Post-substitution of magnesium at Ca(I) of nano-hydroxyapatite surface for highly efficient and selective removal of radioactive (90)Sr from groundwater. *Chemosphere*. 2022;295:133874. doi:10.1016/j.chemosphere.2022.133874
22. Mahdavinia GR, Hosseini R, Darvishi F, Sabzi M. The release of cefazolin from chitosan/polyvinyl alcohol/sepiolite nanocomposite hydrogel films. *Iran Polym J*. 2016;25(11):933–943. doi:10.1007/s13726-016-0480-2
23. Abdel-Mohsen AM, Aly AS, Hrdina R, Montaser AS, Hebeish A. Eco-Synthesis of PVA/Chitosan Hydrogels for Biomedical Application. *J Polym Environ*. 2011;19(4):1005–1012. doi:10.1007/s10924-011-0334-0
24. Figueroa-Pizano MD, Vélaz I, Peñas FJ, et al. Effect of freeze-thawing conditions for preparation of chitosan-poly (vinyl alcohol) hydrogels and drug release studies. *Carbohydr Polym*. 2018;195:476–485. doi:10.1016/j.carbpol.2018.05.004
25. Yang T, Xie P, Wu Z, et al. The Injectable Woven Bone-Like Hydrogel to Perform Alveolar Ridge Preservation With Adapted Remodeling Performance After Tooth Extraction. *Front Bioeng Biotechnol*. 2020;8:119. doi:10.3389/fbioe.2020.00119
26. Liuyun J, Yubao L, Chengdong X. Preparation and biological properties of a novel composite scaffold of nano-hydroxyapatite/chitosan/carboxymethyl cellulose for bone tissue engineering. *J Biomed Sci*. 2009;16(1):65. doi:10.1186/1423-0127-16-65
27. Ciolacu DE, Rusu D, Darie-Niţă RN, Tîmpu D, Ciolacu F. Influence of Gel Stage from Cellulose Dissolution in NaOH-Water System on the Performances of Cellulose Allomorphs-Based Hydrogels. *Gels*. 2022;8(7):410. doi:10.3390/gels8070410
28. Ma Z, Nelson DM, Hong Y, Wagner WR. Thermally responsive injectable hydrogel incorporating methacrylate-polylactide for hydrolytic lability. *Biomacromolecules*. 2010;11(7):1873–1881. doi:10.1021/bm1004299

29. Huang K, Wu J, Gu Z. Black Phosphorus Hydrogel Scaffolds Enhance Bone Regeneration via a Sustained Supply of Calcium-Free Phosphorus. *ACS Appl Mater Interfaces*. 2019;11(3):2908–2916. doi:10.1021/acsami.8b21179
30. Iconaru SL, Ciobanu CS, Predoi G, et al. Biological and Physico-Chemical Properties of Composite Layers Based on Magnesium-Doped Hydroxyapatite in Chitosan Matrix. *Micromachines*. 2022;13(10):1574. doi:10.3390/mi13101574
31. Predoi D, Iconaru SL, Predoi MV, Stan GE, Synthesis BN. Characterization, and Antimicrobial Activity of Magnesium-Doped Hydroxyapatite Suspensions. *Nanomaterials*. 2019;9(9):1295. doi:10.3390/nano9091295
32. Zhao F, Yao D, Guo R, Deng L, Dong A, Zhang J. Composites of Polymer Hydrogels and Nanoparticulate Systems for Biomedical and Pharmaceutical Applications. *Nanomaterials*. 2015;5(4):2054–2130. doi:10.3390/nano5042054
33. Gaharwar AK, Peppas NA, Khademhosseini A. Nanocomposite hydrogels for biomedical applications. *Biotechnol Bioeng*. 2014;111(3):441–453. doi:10.1002/bit.25160
34. Campiglio CE, Contessi Negrini N, Farè S, Draghi L. Cross-Linking Strategies for Electrospun Gelatin Scaffolds. *Materials*. 2019;12(15):2476. doi:10.3390/ma12152476
35. Desfrançois C, Auzély R, Texier I. Lipid Nanoparticles and Their Hydrogel Composites for Drug Delivery: a Review. *Pharmaceuticals*. 2018;11(4):118. doi:10.3390/ph11040118
36. Bao W, Li M, Yang Y, et al. Advancements and Frontiers in the High Performance of Natural Hydrogels for Cartilage Tissue Engineering. *Front Chem*. 2020;8:53. doi:10.3389/fchem.2020.00053
37. Eslahi N, Abdorahim M, Simchi A. Smart Polymeric Hydrogels for Cartilage Tissue Engineering: a Review on the Chemistry and Biological Functions. *Biomacromolecules*. 2016;17(11):3441–3463. doi:10.1021/acs.biomac.6b01235
38. Gadjanski I. Recent advances on gradient hydrogels in biomimetic cartilage tissue engineering. *F1000Research*. 2017;6:F1000 Faculty Rev–2158. doi:10.12688/f1000research.12391.2
39. El-Meliegy E, Abu-Elsaad NI, El-Kady AM, Ibrahim MA. Improvement of physico-chemical properties of dextran-chitosan composite scaffolds by addition of nano-hydroxyapatite. *Sci Rep*. 2018;8(1):12180. doi:10.1038/s41598-018-30720-2
40. Johanes M, Gupta M. An Investigation into the Potential of Turning Induced Deformation Technique for Developing Porous Magnesium and Mg-SiO(2) Nanocomposite. *Materials*. 2023;16(6):2463. doi:10.3390/ma16062463
41. Murugan S, Parcha SR. Fabrication techniques involved in developing the composite scaffolds PCL/HA nanoparticles for bone tissue engineering applications. *J Mater Sci Mater Med*. 2021;32(8):93. doi:10.1007/s10856-021-06564-0
42. Kakuta A, Tanaka T, Chazono M, et al. Effects of micro-porosity and local BMP-2 administration on bioresorption of β-TCP and new bone formation. *Biomater Res*. 2019;23:12. doi:10.1186/s40824-019-0161-2
43. Chiulan I, Frone AN, Brandabur C, Panaitescu DM. Recent Advances in 3D Printing of Aliphatic Polyesters. *Bioengineering*. 2017;5(1):2. doi:10.3390/bioengineering5010002
44. Singelyn JM, Christman KL. Modulation of material properties of a decellularized myocardial matrix scaffold. *Macromol Biosci*. 2011;11(6):731–738. doi:10.1002/mabi.201000423
45. Amante C, Andretto V, Rosso A, et al. Alginate-pectin microparticles loaded with nanoemulsions as nanocomposites for wound healing. *Drug Delivery Transl Res*. 2023;13(5):1343–1357. doi:10.1007/s13346-022-01257-9
46. Xu X, Liu Y, Fu W, et al. Poly(N-isopropylacrylamide)-Based Thermoresponsive Composite Hydrogels for Biomedical Applications. *Polymers*. 2020;12(3):580. doi:10.3390/polym12030580
47. Bhowmick A, Pramanik N, Mitra T, Gnanamani A, Das M, Kundu PP. Mechanical and biological investigations of chitosan-polyvinyl alcohol based ZrO2 doped porous hybrid composites for bone tissue engineering applications. *New J Chem*. 2017;41(15):7524–7530. doi:10.1039/c7nj01246b
48. Liu J, Yu S, Qu W, Jin Z, Zhao K. Self-Assembly of Soluble Chitosan Derivatives Nanoparticles for Vaccine: synthesis, Characterization and Evaluation. *Polymers*. 2021;13(23):4097. doi:10.3390/polym13234097
49. Song M, Yu B, Kim S, et al. Clinical and Molecular Perspectives of Reparative Dentin Formation: lessons Learned from Pulp-Capping Materials and the Emerging Roles of Calcium. *Dental Clin North Am*. 2017;61(1):93–110. doi:10.1016/j.cden.2016.08.008
50. Nie X, Zhang X, Lei B, Shi Y, Yang J. Regulation of Magnesium Matrix Composites Materials on Bone Immune Microenvironment and Osteogenic Mechanism. *Front Bioeng Biotechnol*. 2022;10:842706. doi:10.3389/fbioe.2022.842706
51. Qi H, Liu Y, Wu L, et al. Mg-HA-C/C Composites Promote Osteogenic Differentiation and Repair Bone Defects Through Inhibiting miR-16. *Front Bioeng Biotechnol*. 2022;10:838842. doi:10.3389/fbioe.2022.838842
52. Li D, Yu K, Xiao T, et al. LOC103691336/miR-138-5p/BMPR2 axis modulates Mg-mediated osteogenic differentiation in rat femoral fracture model and rat primary bone marrow stromal cells. *J Cell Physiol*. 2019;234(11):21316–21330. doi:10.1002/jcp.28736
53. Chhatri A, Bajpai J, Bajpai AK. Designing polysaccharide-based antibacterial biomaterials for wound healing applications. *Biomatter*. 2011;1(2):189–197. doi:10.4161/biom.19005
54. Habibovic P, Barrere F, van Blitterswijk C, de Groot K, Layrolle P. Biomimetic hydroxyapatite coating on metal implants. *J Am Ceram Soc*. 2002;85(3):517–522. doi:10.1111/j.1151-2916.2002.tb00126.x